Dispersion Characteristics of One-Dimensional Photonic Band Gap Structures Composed of Metallic Inclusions

by

Maryam Khodami

A thesis submitted to the
Faculty of Graduate and Postdoctoral Studies
In partial fulfillment of the requirements for the degree of

Master of Applied Science

in

Electrical and Computer Engineering

Ottawa-Carleton Institute for Electrical and Computer Engineering

Department of Electrical Engineering and Computer Science
Faculty of Engineering
University of Ottawa

Ottawa, Ontario, Canada, July 2012

Abstract

An innovative approach for characterization of one dimensional Photonic Band Gap structures comprised of metallic inclusions (*i.e.* subwavelength dipole elements or resonant ring elements) is presented. Through an efficient S- to T-parameters conversion technique, a detailed analysis has been performed to investigate the variation of the dispersion characteristics of 1-D PBG structures as a function of the cell element configuration. Also, for the first time, the angular sensitivity of the structure has been studied in order to obtain the projected band diagrams for both TE and TM polarizations.

Polarization sensitivity of the subwavelength cell element is exploited to propose a novel combination of elements which allows achieving PBGs with simultaneous frequency and polarization selectivity. The proposed approach demonstrates that the dispersion characteristic of each orthogonal polarization can be independently adjusted with dipole elements parallel to that same polarization. Generally, the structure has potential applications in orthomode transducer, and generally whenever the polarization of the incoming signal is to be used as a means of separating it from another signal in the same frequency band that is of orthogonal polarization.

The current distribution and the resonance behavior of the ring element is studied and the effect of resonance on dispersion characteristics of 1-D PBGs composed of rings is investigated for the first time, for both individual and coupled rings. Interestingly, it is observed that 1-D PBG composed of resonant elements consistently has a bandgap around the resonant frequency of the single layer structure.

Acknowledgments

First and for most, I would like to express my gratitude and appreciation to my thesis supervisor, Professor Mustapha C.E. Yagoub, and my thesis co-supervisor, Professor Jafar Shaker, for their support and encouragement during my Master's study. This work would not have been possible without their guidance and help. I am also grateful to them for providing financial support which made this work possible.

I would also like to thank Professor D. McNamara and Professor L. Roy for their acceptance to be in the examination committee.

Last, but not least, I offer my deepest gratitude to my parents, for their love, support and patience.

Maryam Khodami,

Ottawa, July 2012

Acronyms

PBG	Photonic Band Gap
TMM	Transfer Matrix Method
TE	Transverse Electric
TM	Transverse Magnetic
SRR	Split Ring Resonator

List of Symbols

A, A_{ij}	Transfer Matrix Element
$\boldsymbol{B}$	Electric field vector
B	Transfer Matrix Element
c	Light velocity in vacuum
C	Transfer Matrix Element
$\boldsymbol{D}$	Displacement field vector
D	Transfer Matrix Element
$\boldsymbol{E}$	Electric field vector
$\boldsymbol{H}$	Magnetic field vector
k	Wave vector
n	Refractive index
r	Distance
S_{ij}	Scattering matrix elements
t	Time
T	Transfer matrix
$\boldsymbol{J}$	Current density vector
$\boldsymbol{\rho}$	Free charge vector
ε_0	Vacuum permittivity
ε	Relative permittivity
μ_0	Vacuum permeability
λ	Wavelength
ω	Angular frequency
μ	Relative permeability

Table of Contents

1 INTRODUCTION 1

1.1 –PHOTONIC BAND GAP STRUCTURE CONCEPTS 1

1.2– MOTIVATION 2

1.3 – THESIS CONTRIBUTIONS 3

1.3 –THESIS OBJECTIVES AND OVERVIEW 3

1.4 – REFERENCES OF CHAPTER 1 5

2 WAVE PROPAGATION IN ONE DIMENSIONAL PERIODIC DIELECTRIC MEDIA 7

2.1 – INTRODUCTION 7

2.2 – WAVE EQUATION 7

2.3 – TRANSLATIONAL SYMMETRY, BLOCH STATES AND BRILLOUIN ZONE 10

2.4– PHOTONIC BAND STRUCTURES 11

2.5 – MULTILAYER FILM 13

2.5.1 –Preiliminary Remarks: Bragg Condition 14

2.5.2– Wave Propagation in Periodic Layered Media: Transfer Matrix Method 15

2.5.3– Bloch Wave and Band Structure 19

2.5.4– Microwave Circuit Analysis 23

2.5.5– Transmission Matrix Element and Band Structures of Stratified Medium: Revisited 25

2.6 – CONCLUSION 28

2.7 – REFERENCES OF CHAPTER 2 29

3 DISPERSION CHARACTRISTICS OF 1-D PBG STRUCTURES COMPOSED OF SUBWAVELENGTH DIPOLE ELEMENTS 30

3.1 – INTRODUCTION 30

3.2 – THEORY 31

3.3 – DISPERSION CHARECTRISTICS AS FUNCTION OF CELL ELEMENT CONFIGURATION 32

3.4 – ANGULAR SENSITIVITY 37

3.5 – SIMULTANOUS POLARIZATION AND FREQUENCY SELECTIVITY 39

3.6 – EFFECT OF SUBSTRATE 43

3.7 – OTHER CONFIGURATIONS: METAL STRIP 47

3.8 – CONCLUSION 48
3.9 – REFERENCES OF CHAPTER 3 49

4 DISPERSION CHARACTERISTICS OF 1-D PBG STRUCTURES COMPOSED OF SPLIT RING RESONATOR ELEMENTS 50

4.1 – INTRODUCTION 50
4.2 – THEORY 50
4.3 – INDIVIDUAL RING 52
4.3.1 Resonance behaviour, Ring Current and dispersion characteristic 52
4.3.2 Parametric Study 55
4.4 – COUPLED RINGS 61
4.4.1 180^o rotation 62
4.4.2 90^o rotation 66
4.5 – CONCLUSION 69
4.6 – REFRENCES OF CHAPTER 4 70

5 GENERAL CONCLUSIONS AND PERSPECTIVES 72

5.1 – SUMMARY 72
5.2 – PERSPECTIVES AND FUTURE WORK 73

APPENDIX A 74

List of Figures

Fig. 2.1 A system with discrete periodicity in *y* direction 11

Fig. 2.2 Schematic of 1- 2- and 3-D crystal lattices 13

Fig. 2.3 The multilayer film as a one-dimensional photonic band gap material. 14

Fig. 2.4 A one dimensional periodic medium. The coordinate system and light rays refracting and propagating through a stack are shown 15

Fig. 2.5 Photonic band structure of a typical one-dimensional photonic crystal for $k_y = 0$. The frequency is normalized as $\omega\Delta/2\pi c$ and the wave number *K* is normalized as $K\Delta/\pi$. 23

Fig. 2.6 Two port network with the representation of incoming and outgoing waves 24

Fig. 2.7 Geometry of the multilayer film structure 26

Fig. 2.8 Photonic band structure of a typical one dimensional photonic crystal for $k_y = 0$. The frequency is normalized as $\omega\Delta/2\pi c$ and the wave number *K* is normalized as $K\Delta/\pi$. 27

Fig.2.9 S parameters for cascading of 2 layers of multilayer film, obtained by HFSS simulation and multiplyingT matrices. 27

Fig. 3.1-a Three dimensional geometry of single cell of the PBG structure. 32

Fig. 3.1-b Top view of the PBG structure in the transverse *xoy* plane. The notation shown in this figure for the geometrical parameters will be used throughout this chapter. The same structure shown in (b) is repeated along *z* axis with period *D*. 32

Fig. 3.2 S-parameters of the single layer of the structures described in Table 3.1. 33

Fig. 3.3-a Normalized propagation constant 34

Fig. 3.3-b Normalized attenuation constant.The legend refers to the structures described in Table 3.1. 34

Fig. 3.4-a Scattering response of the cascade of 15 layers of structures listed in Table 3.1: Reflectance 35

Fig. 3.4-b Scattering response of the cascade of 15 layers of structures listed in Table 3.1: Transmittance 35

Fig. 3.5 Dispersion curve for three different separations between the consecutive layers (*D*). 36

Fig. 3.6 Dispersion curve for two different lattice widths. 36
Fig. 3.7-a Dispersion curves for different angle of propagations for the structure shown in Fig. 3.1 for TM Polarization 38
Fig. 3.7-b Dispersion curves for different angle of propagations for the structure shown in Fig. 3.1 for TE polarization..... 38
Fig. 3.8 Projected Band Diagram for the structure shown in Fig. 3.1 for TM polarization (right panel) and TE polarization (left panel). 39
Fig. 3.9 Dispersion characteristics of the structure shown in Fig. 3.1 when T_x=1mm, T_y=1mm, l=0.9mm, and w=0.1mm for normal propagating mode with the E-field parallel or normal to the dipole..... 41
Fig. 3.10 Three dimensional geometry of single cell of PBG structure composed of cascade connection of dipoles with orthogonal orientation..... 41
Fig. 3.11 Dispersion curve for the structure of Fig. 3.10 for normal propagating modes with E-field polarization parallel to dipoles on layer A. The solid curve in this figure represents the case that just layer *A* is present in Fig. 3.10, while the dashed curve represents the case that both layers *A* and *B* are present. 41
Fig. 3.12 Dispersion curve for the structure of Fig. 3.10 for normal propagating modes with E-field polarization parallel to dipoles on layer B. The solid curve in this figure illustrates the case that just layer *B* is present in Fig. 3.10, while the dashed curve represents the case that both layers *A* and *B* are present. 42
Fig. 3.13 Three dimensional geometry of single cell of PBG structure composed of cascade connection of dipoles with orthogonal orientation..... 42
Fig. 3.14 Dispersion curve for the structure of Fig. 3.13 when modal polarization matches the dipoles on layer A. The solid curve in this figure illustrates the case that just layer *A* is present in Fig 3.13, while the dashed curve represents the case that both layers *A* and *B* are present. 42
Fig. 3.15 Dispersion curve for the structure of Fig. 3.13 when modal polarization matches the dipoles on layer B. The solid curve in this figure illustrates the case that just layer *B* is present in Fig 3.13, while the dashed curve represents the case that both layers *A* and *B* are present. 43
Fig. 3.16 Dispersion curve for three different separations between the consecutive layers (*D*) for E field polarization parallel or normal to the dipole. 44

Fig. 3.17 Dispersion curve for normal polarization and bare substrate case. 45
Fig. 3.18 Three dimensional representation of a single cell of PBG structure composed of cascade connection of dipoles with orthogonal orientation. The substrate is present in this case. 45
Fig. 3.19 Dispersion curve for the structure of Fig. 3.18 when modal polarization matches the dipoles on layer A. The solid curve in this figure illustrates the case that just layer *A* is present in Fig 3.18, while the dashed curve represents the case that both layers *A* and *B* are present 46
Fig. 3.20 Dispersion curve for the structure of Fig. 3.17 when modal polarization matches the dipoles on layer A. The solid curve in this figure illustrates the case that just layer *A* is present in Fig 3.17, while the dashed curve represents the case that both layers *A* and *B* are present 46
Fig 3.21 Fabry-Perot phenomena in metal strip 47
Fig. 4.1-a Three dimensional geometry of single cell of the PBG structure. 51
Fig. 4.1-b Top view of the PBG structure in the transverse plane. 51
Fig. 4.2 Transmission coefficient for individual ring (a) *E* field parallel to the gap (b) *E* filed normal to the gap 53
Fig. 4.3 Current distribution for *E* field parallel to the gap at (a) 10.4GHz (b) 28.7 GHz (b) *E* field normal to the gap at 21.45 53
Fig. 4.4-a Dispersion characteristics for 1-D PBG structure composed of ring element for *E* field polarization parallel to the gap 54
Fig. 4.4-b Dispersion characteristics for 1-D PBG structure composed of ring element for *E* field polarization normal to the gap 54
Fig. 4.5 Scattering response of the cascade of 15 layers of 1-D PBG composed of SRR for *E* field polarization parallel to the gap 54
Fig. 4.6 Scattering response of the cascade of 15 layers of 1-D PBG composed of SRR for *E* field polarization normal to the gap 55
Fig. 4.7-a Transmission coefficient for different cell size for symmetric of electric field direction 56
Fig. 4.7-b Transmission coefficient for different cell size for asymmetric of electric field direction 56
Fig. 4.8-a Dispersion characteristics as a function of cell element size for E field polarization normal to the gap 57

Fig. 4.8-b Dispersion characteristics as a function of cell element size for E field polarization parallel to the gap 57
Fig. 4.9-a Dispersion curve for three different separation between the consecutive layers for E field polarization normal to the gap 58
Fig. 4.9-b Dispersion curve for three different separation between the consecutive layers for E field polarization parallel to the gap 58
Fig. 4.10-b Dispersion curve for different angle of propagation for the structure shown in Fig. 4.1-b for TM polarization 60
Fig. 4.10-b Dispersion curve for different angle of propagation for the structure shown in Fig. 4.1-b for TE polarization 60
Fig. 4.11-a Projected Band Diagram for the structure shown in Fig. 4.1(b) for TM polarization in *yoz* plane 61
Fig. 4.11-b Projected Band Diagram for the structure shown in Fig. 4.1(b) for TE polarization in *yoz* plane 61
Fig. 4.12-a Electric field direction normal to the gap parallel to the gap 62
Fig. 4.12-b Electric field direction parallel to the gap 62
Fig. 4.13 Transmission coefficient for *E* field normal to the gap 63
Fig. 4.14 Current distribution for *E* field normal to the gap at 21.6 GHz 63
Fig. 4.15 Transmission coefficient for *E* field parallel to the gap 64
Fig. 4.16 Current distribution for *E* field parallel to the gap at 10.25 GHz 64
Fig. 4.17 Current distribution for *E* field parallel to the gap at 29.8 GHz 65
Fig. 4.18-a Dispersion characteristics for 180 degree rotated rings for E field normal to the gap 65
Fig. 4.18-b Dispersion characteristics for 180 degree rotated rings for E field parallel to the gap 66
Fig. 4.19 Electric field direction with respect to the ring locations 66
Fig 4.20 Transmission coefficient for *E* field configuration of Fig. 4.19. 67
Fig. 4.21 Current distribution for E field polarization normal to the lower ring at (a) 9.95 GHz (b) 21.55 GHz (c) 29.8 GHz 68
Fig. 4.22 Dispersion characteristics for 90 degree rotated rings 69

List of Tables

Table 3.1 Geometrical parameters for dipole structure shown in Fig. 3.1. 33

Chapter 1

Introduction

1.1 Photonic Band Gap Concepts

Photonic Band Gap structures (PBGs) have been the subject of intense research in recent years due to their capability to control the flow of electromagnetic waves [1]. Photonic Band Gap (*i.e*; counterpart of electronic band gap in semiconductors) is caused by Bragg Diffraction [2] and corresponds to a frequency band across which the propagation of a given polarization along a given direction is forbidden. Therefore, a complete photonic band gap refers to a frequency band throughout which no mode is allowed to propagate through the structure regardless of its polarization or angle of incidence.

Existence of PBG allows confinement of electromagnetic modes that can be used for a multitude of applications, such as novel filter designs [3], superprism effect and negative refraction [4], suppression of surface waves [5], and fabrication and design of guided wave structures [6]. Many of these applications are based on the frequency and bandwidth of the gap.

The history of studying wave propagation in periodic media dates back to the pioneering works by Lord Rayleigh in 1887. He investigated a crystalline mineral with periodic twining planes [7] and showed that this structure, which is a "one-dimensional photonic crystal", has a narrow band gap throughout which, light is not allowed to propagate. This gap is angular sensitive, because of the fact that light is subjected to different periodicities when it is propagating at non-normal angle of incidence. Lord Rayleigh used Mathieu differential equations to solve the problem of wave propagation in such a medium [8]. Later in 1928, Bloch used the results of partial differential equations with periodic coefficient and found a solution for the wave propagation in layered media, which is called Bloch waves. At that time, periodic multilayer film was broadly investigated, because of its application in filters, beam splitters, and polarizers. Later in 1960's, the solution of the wave equation in periodic media resulted in further developments in this field. In 1970's passive and active thin film

optical waveguides and the fabrication of solid state grating led to application of 1-D gratings in the context of thin films and fibers [8].

Although multilayer films was the subject of intense research over the following century, it was only 100 years later in 1987, when Yablonovitch [9] and John [10] introduced the concepts of 2D and 3D omnidirectional photonic bandgaps. This generalization, led to many further developments in the, theory, application, and fabrication of crystals.

1.2 Motivation

One-dimensional (1-D) PBG structures can be classified into three main groups. One type is 1-D periodic multilayer film which is composed of consecutive arrangement of thin dielectric layers [11]. In this type of structures, permittivity varies periodically in space, which results in the existence of a band gap along the direction of stratification. While a complete photonic band gap only occurs in 3D lattices, its 1D and 2D counterparts which are much easier to fabricate, have been studied intensively and the properties of stop-band and pass-band of such structures have been broadly investigated in the literature [12].

Another implementation of 1-D photonic band gap structures is composed of lumped elements that are connected by a transmission line. This type is used to implement periodically loaded transmission line networks with anti-parallel group and phase velocities and have been used as the building block of Metamaterials [13].

The other type of 1-D photonic band gap materials, which is the subject of this thesis, is a cascade connection of layers that are comprised of inclusions imbedded within a host medium [14]. Multiple reflection between consecutive layers results in Bragg diffraction phenomenon which leads to the emergence of band gap in such structures. Frequency band and width of the band gap can be adjusted by modifying the scattering parameters of each constituent layer.

A wide variety of numerical and analytical methods are available for computing the band structure of PBGs composed of dielectric layers [15-17]. However, in the case of PBGs composed of inclusions (i.e. dipole or ring elements), no closed-form analytic expression is currently available to calculate the dispersion characteristics. That has motivated the use of scattering matrix to transmission matrix conversion technique, as presented in this work, for numerical calculation of the dispersion characteristics. In this approach, scattering parameters of a single layer are calculated using full wave software HFSS [18]. Then, the conversion of

scattering matrix to transmission matrix is used to compute the band diagram of the 1-D periodic structure [19, 20].

1.3 Thesis Contributions

The main contributions of this thesis are listed below. In fact, *for the first time*:

- A detailed parametric study is performed to investigate the variation of dispersion curve vs. design parameters for 1-D PBG structure composed of dipoles [21].
- Angular dependence of the dispersion of 1-D PBG structures comprised of layers of dipoles is investigated and related projected band diagrams are presented [21].
- A novel PBG structure with simultaneous frequency and polarization selectivity is proposed [22].
- Dispersion characteristics of individual and coupled rings are investigated and relationship between resonance and structure band gap is studied.
- A detailed parametric study is performed to investigate the variation of dispersion curve vs. design parameters for 1-D PBG structure, composed of individual rings
- Angular dependence of 1-D PBG structure, composed of individual rings, is investigated and related projected band diagrams are presented.

1.4 Thesis Objectives and Overview

It is necessary to understand that the problem at hand (wave propagation in periodic media) is basically an eigenvalue problem and it is possible to solve this problem for periodic multilayer film through an analytic method based on transfer matrix technique. This is the subject of Chapter 2. Beyond that, the pertinent microwave circuit theory and scattering matrix to transmission matrix conversion technique that is used in the calculation of band structure for 1-D multilayer film is presented and discussed in this chapter.

The subject of Chapter 3 is the dispersion characteristics of 1-D PBG structures composed of subwavelength dipole elements. Based on the method developed in Chapter 2, a detailed analysis is performed to investigate the variation of dispersion curve vs. design parameters for 1-D PBGs composed of dipoles. Also the angular dependence of the dispersion characteristics is studied. Furthermore, a novel PBG structure with simultaneous frequency and polarization selectivity is proposed in this chapter.

Following the procedure of Chapter 3, dispersion characteristics of 1-D PBG structures composed of resonant open ring elements are discussed in Chapter 4. A detailed analysis is performed to investigate the variation of dispersion curve vs. design parameters. Also the angular dependence of the structure is investigated. The current distribution on the ring surface and resonance behaviour of individual and coupled rings (with 90^{o} or 180^{o}rotation with respect to each other) are discussed in this chapter. The thesis will be closed with general conclusions.

1.5 References for Chapter 1

1. J.D. Joannopoulos, S.G. Johnson, J.N. Winn, and R.D. Meade, *Photonic Crystals Molding the Flow of Light*, Princeton University Press, Princeton, 2008
2. S.G. Romanov, D.N. Chigrin, V.G. Solovyev, T. Maka, N. Gaponik, A. Eychmüller, A.L. Rogach, and C.M. Sotomayor Torres, "Light emission in a directional photonic band gap,"*Phys. Stat. Sol. (a)*,vol. 197, pp. 662– 672, 2003.
3. F. Birbir, J. Shaker, and Y.M.M. Antar, *"*Chebishev bandpass spatial filter composed of strip gratings," *IEEE Trans. Antennas Propag.*, vol. 56, pp. 3707-3713, 2008.
4. H. Kosaka*et al*., "Superprism phenomena in photonic crystals," *Phys. Rev. B*, vol. 58, pp.10096-19999, 1998.
5. H.Contopanagos, L. Zhang, and N.G. Alexopoulos, "Thin frequency selective lattices integrated in novel compact MIC, MMIC and PCA architectures," *IEEE Trans. Antennas Propag*., vol. 94, pp. 1936-1948, 1998.
6. A. Adibi, Y. Xu, R.K. Lee, A. Yariv, and A. Scherer, "Properties of the slab modes in photonic crystal optical waveguides,"*J. Lightwave Tech*, vol. 18, pp. 1554-1564,2000.
7. http://ab-initio.mit.edu/photons/tutorial/photonic-intro.pdf, accessed June 2012.
8. C. Elachi, "Waves in active and passive periodic structures: A review," *Proc. of the IEEE*, vol. 64, pp. 1666-1698, 1976.
9. E. Yablonovitch, Inhibited Spontaneous Emission In solid State Physics and Electronics, Phys. Rev. Lett. 58, pp. 2059-2062, 1987.
10. S. John, "Strong localization of photons in certain disordered dielectric superlattices," *Phys. Rev. Lett*. vol. 58, pp. 2486-2489, 1987.
11. D.N. Chigrin, A.V. Lavrinenko, D.A. Yarotsky, and S.V. Gaponenko, "All-dielectric one-dimensional periodic structures for total omnidirectional reflection and partial spontaneous emission control," *J. Lightwave Tech*., vol. 17, pp. 2018-2024, 1999.
12. D.N. Chigrin, and C.M. Sotomayor Torres, "Periodic thin-film interference filters as one-dimensional photonic crystals," *Opt. Spectrosc*, pp. 1-6, 2001.
13. O.F. Siddiqui, M. Mojahedi, and G.V. Eleftheriades, "Periodically loaded transmission line with effective negative refractive index and negative group velocity," *IEEE Trans. Antennas Propag.*, vol. 51, pp. 2619-2625, 2003.

14. C.A. Kyriazidou, H.F. Contopanagos, W.M. Merrill, and N.G. Alexópoulos, "Artificial versus natural crystals: effective wave impedance of printed photonic bandgap materials,"*IEEE Trans. Antennas Propag.*, vol. 48, pp. 95-106, 2000.
15. L.C. Botten, N.A. Nicorovici, R.C. McPhedran, C. Martijn de Sterke, and A.A. Asatryan, "Photonic band structure calculations using scattering matrices," *Phys. Rev. E*, vol.64, pp. 046603/1-046603/18,2001.
16. W. Axmann and P. Kuchment, "An efficient finite element method for computing spectra of photonic and acoustic band-gap materials: I. Scalar case," *J. Comput. Phys*. vol. 150, pp. 468–481,1999.
17. J.B. Pendry and A. MacKinnon, "Calculation of photon dispersion relations," *Phys. Rev. Lett*. vol. 69, pp. 2772–2775, 1992.
18. HFSS ver. 12. Pittsburgh, PA, Ansoft Corp.
19. R.S. Kshetrimayumand L. Zhu, "Guided wave characteristics of waveguide based periodic structures loaded with various FSS strip layers," *IEEE Trans. Antennas Propag.*, vol. 53, pp. 120-124, 2005.
20. A. Akbarzadeh-Jahromi, M. Tayarani, and M. Khalaj-Amirhosseini, "Periodically loaded rectangular wave guide with FSS Strip layer supporting wideband Backward Wave,"*Int. J. Electrical, Electronics and Computer System*, vol. 04, pp. 20-23, 2011.
21. M. Khodami, J. Shaker, M.C.E. Yagoub, "Parametric study of 1-D PBG structures composed of subwavelength dipole elements," (Submitted)
22. M. Khodami, J. Shaker, M.C.E. Yagoub, "Dispersion characteristics of 1-D PBG structures composed of subwavelength dipole elements," (Submitted)

Chapter 2

Wave Propagation in One Dimensional Periodic Dielectric Media

2.1 Introduction

In this chapter we begin our study of photonic band gap structures by introducing the problem as an eigenvalue problem. A brief presentation of photonic bandgaps, Bloch states and Brillouin Zones is given in the next three sections, following the procedure and notation proposed in [1]. This discussion cannot be considered as a complete formulation on this topic, but it is sufficient to understand the problem at hand. The reader is referred to [1-3], for further details.

A thorough discussion on transfer matrix formulation is given in section 2.5 and the analytical expression which describes wave propagation in multilayer film structures is derived. The dispersion diagram is obtained for this structure based on the derived formula.

At the end, microwave circuit analysis of periodic structure is discussed and another approach based on the conversion of scattering parameters to transmission matrix element is developed to obtain the dispersion diagram of 1-D periodic multilayer film.

2.2 Wave Equation

In order to solve the problem of wave propagation in a periodic dielectric medium, one can begin with Maxwell equations:

$$\begin{aligned} \nabla \cdot \boldsymbol{B} &= 0 \\ \nabla \times \boldsymbol{E} + \frac{\partial \boldsymbol{B}}{\partial t} &= 0 \\ \nabla \cdot \boldsymbol{D} &= \rho \\ \nabla \times \boldsymbol{H} - \frac{\partial \boldsymbol{D}}{\partial t} &= \boldsymbol{J} \end{aligned} \tag{2-1}$$

in which $\boldsymbol{E}$ and $\boldsymbol{H}$ are electric and magnetic fields, $\boldsymbol{D}$ and $\boldsymbol{B}$ are the displacement and the magnetic induction fields, and ρ and $\boldsymbol{J}$ are the free charge and current density. In this set of equations, $\boldsymbol{D}$ relates to $\boldsymbol{E}$, and $\boldsymbol{B}$ relates to $\boldsymbol{H}$ through constitutive relations. For a linear, isotropic, non dispersive material [1] the constitutive relations have the form:

$$\begin{aligned} \boldsymbol{D}(\boldsymbol{r}) &= \varepsilon_0 \varepsilon(\boldsymbol{r}) \boldsymbol{E}(\boldsymbol{r}) \\ \boldsymbol{B}(\boldsymbol{r}) &= \mu_0 \mu(\boldsymbol{r}) \boldsymbol{H}(\boldsymbol{r}) \end{aligned} \tag{2-2}$$

in which $\varepsilon(\boldsymbol{r})$ and $\mu(\boldsymbol{r})$ are relative electric permittivity and magnetic permeability, and ε_0 and μ_0 are permittivity and permeability of vacuum, respectively. For most dielectric materials $\mu(\boldsymbol{r})$ is very close to unity. In this case, by inserting the constitutive equations into the Maxwell's equations, the following can be written:

$$\begin{aligned} \nabla \cdot \boldsymbol{H}(\boldsymbol{r}, t) &= 0 \\ \nabla \times \boldsymbol{E}(\boldsymbol{r}, t) + \mu_0 \frac{\partial \boldsymbol{H}(\boldsymbol{r}, t)}{\partial (t)} &= 0 \\ \nabla \cdot [\varepsilon(\boldsymbol{r}) \boldsymbol{E}(\boldsymbol{r}, t)] &= 0 \\ \nabla \times \boldsymbol{H}(\boldsymbol{r}, t) - \varepsilon_0 \varepsilon(\boldsymbol{r}) \frac{\partial \boldsymbol{E}(\boldsymbol{r}, t)}{\partial (t)} &= 0 \end{aligned} \tag{2-3}$$

In general both $\boldsymbol{E}$ and $\boldsymbol{H}$ are functions of time and space. Because of the linearity of the Maxwell's equations the time dependency can be separated from the spatial dependency, by expanding the fields into a set of harmonic modes. Based on that, a harmonic mode can be written as a spatial pattern times a complex exponential:

$$\begin{aligned} \boldsymbol{H}(\boldsymbol{r}, t) &= \boldsymbol{H}(\boldsymbol{r}) e^{j\omega t} \\ \boldsymbol{E}(\boldsymbol{r}, t) &= \boldsymbol{E}(\boldsymbol{r}) e^{j\omega t} \end{aligned} \tag{2-4}$$

To find the equation governing the mode profiles for a given angular frequency ω, equation (2-4) is inserted into equation (2-3), and the following condition is obtained:

$$\nabla \cdot \boldsymbol{H}(\boldsymbol{r}) = 0$$
$$\nabla \cdot [\varepsilon(\boldsymbol{r})\boldsymbol{E}(\boldsymbol{r})] = 0$$

(2-5)

The two curl equations relate $\boldsymbol{E}(\boldsymbol{r})$ to $\boldsymbol{H}(\boldsymbol{r})$:

$$\nabla \times \boldsymbol{E}(\boldsymbol{r}) - j\omega\mu_0 \boldsymbol{H}(\boldsymbol{r}) = 0$$
$$\nabla \times \boldsymbol{H}(\boldsymbol{r}) + j\omega\varepsilon_0\varepsilon(\boldsymbol{r})\boldsymbol{E}(r) = 0$$

(2-6)

By combining the two equations and eliminating $\boldsymbol{E}(\boldsymbol{r})$, an equation entirely in $\boldsymbol{H}(\boldsymbol{r})$ can be obtained:

$$\nabla \times \left(\frac{1}{\varepsilon(\boldsymbol{r})}\nabla \times \boldsymbol{H}(\boldsymbol{r})\right) = \left(\frac{\omega}{c}\right)^2 \boldsymbol{H}(\boldsymbol{r})$$

(2-7)

in which *c* is the light velocity in vacuum. This is the "master equation", which can be solved to find the modes of $\boldsymbol{H}(\boldsymbol{r})$. Then the second equation of (2-6) can be used to find $\boldsymbol{E}(\boldsymbol{r})$:

$$\boldsymbol{E}(\boldsymbol{r}) = \frac{j}{\omega\varepsilon_0\varepsilon(\boldsymbol{r})}\nabla \times \boldsymbol{H}(\boldsymbol{r})$$

(2-8)

It is also possible to derive $\boldsymbol{H}(\boldsymbol{r})$ from $\boldsymbol{E}(\boldsymbol{r})$ using the first equation of (2-6):

$$\boldsymbol{H}(\boldsymbol{r}) = \frac{-j}{\omega\mu_0}\nabla \times \boldsymbol{E}(\boldsymbol{r})$$

(2-9)

Equation (2-7) demonstrates an “eigenvalue" problem, in which an operator performs on function $\boldsymbol{H}(\boldsymbol{r})$, and the result is a constant times the original function$\boldsymbol{H}(\boldsymbol{r})$. In this case the function $\boldsymbol{H}(\boldsymbol{r})$ is "eigenfunction" or "eigenvector" of the operator and the multiplicative constant is the "eigenvalue" of the system.

The left side of equation (2-7) can be identified as an operator Θ acting on $\boldsymbol{H}(\boldsymbol{r})$, to make it looks more like a traditional eigenvalue problem. Based on that:

$$\Theta \boldsymbol{H}(\boldsymbol{r}) = \left(\frac{\omega}{c}\right)^2 \boldsymbol{H}(\boldsymbol{r}) \tag{2-10}$$

in which Θ is defined as an operator which takes the curl, then divides by $\boldsymbol{\varepsilon}(\boldsymbol{r})$ and then takes the curl again.

$$\Theta \boldsymbol{H}(\boldsymbol{r}) \triangleq \nabla \times \left(\frac{1}{\varepsilon(\boldsymbol{r})} \nabla \times \boldsymbol{H}(\boldsymbol{r})\right) \tag{2-11}$$

It is worth to note that Θ is a linear operator and any combination of solutions is itself a solution. This operator also has some other special properties: the eigenvalues are real and orthogonal to each other. These properties rely on the fact that the main operator is a special type of operator known as a Hermitian operator**.** The full detail about the properties of such operators can be found in [1].

2.3 Translational symmetry, Bloch States and Brillouin zone

Photonic band gap structures have discrete translational symmetry, which means that they are invariant under translation of distances that are a multiple of some fixed step length. The basic step length is called the lattice constant "*a*" and the basic step vector is called the primitive lattice vector. The dielectric permittivity of a crystal is a periodic function in the form $\varepsilon(\boldsymbol{r}) = \varepsilon(\boldsymbol{r} + a)$for any *a.* By repeating this translation, it can be seen that $\varepsilon(\boldsymbol{r}) = \varepsilon(\boldsymbol{r} + R)$, for any *R* which is an integral multiple of a.

If, for example, the periodic structure of interest has a discrete translational symmetry in *y* direction (Fig. 2.1), one can classify the modes propagating in the structure by considering two different modes with wave vectors k_y and $k_y + 2\pi/a$. By inserting the two modes into master equation (2-7) one can find that these two modes have the same eigenvalue. Generally all of the modes in the form of $k_y + m(2\pi/a)$, where *m* is an integer, form a degenerate set with

the same eigenvalue. Adding any integer multiple of the form $b=2\pi/a$ to k_y leaves the state unchanged. Such a value of b is called the primitive "reciprocal lattice vector".

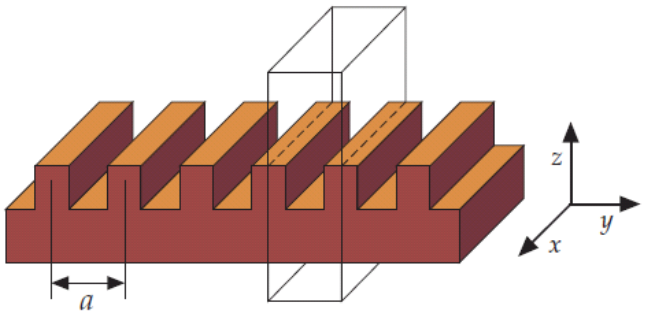

Fig. 2.1. A system with discrete periodicity in *y* direction [1]

In a system with discrete periodicity in the *y* direction, $\boldsymbol{H}$ field depends on *y* which can be stated as a product of a plane wave with a *y*-periodic function. The plane wave factor captures the propagating wave and the periodic factor encapsulates the periodicity of the field. It describes a plane wave in free space, which is modulated by a periodic function because of the periodic lattice:

$$\boldsymbol{H} \propto e^{jk_y y}.u_{k_y} \tag{2-12}$$

This result is known as "Bloch's theorem". In solid-state physics, this form is known as a "Bloch state"[4], and in mechanics as a "Floquet mode" [5].It is worth noting that the Bloch state with wave vector "k_y" and the Bloch state with wave vector "$k_y + mb$", with $b=2\pi/a$, are identical. Based on that, only k_y in the range $-\pi/a < ky < \pi/a$ needs to be considered. This region which includes non-redundant values of k_y is called the "Brillouin zone". The set of wave vectors with $m=0$, is called the "first Brillouin zone". The first Brillouin zone might be redundant if the crystal has some additional symmetries other than translational symmetry (i.e. mirror planes). In this case, the "irreducible Brillouin zone" can be obtained by eliminating these redundant values. For a one dimensional crystal with time reversal symmetry, the irreducible Brillouin zone would be $0 < ky < \pi/a$ [1].

2.4 Photonic Band Structures

According to section 2.3, electromagnetic modes in periodic structures can be written in the form of Bloch states. To solve the problem and obtain $u_k(\boldsymbol{r})$, one could insert the Bloch state into the master equation (2-7):

$$\Theta \boldsymbol{H}_{\mathbf{k}} = \left(\frac{\omega(k)}{c}\right)^2 \boldsymbol{H}_{\boldsymbol{k}}$$

$$\nabla \times \left(\frac{1}{\varepsilon(\boldsymbol{r})} \nabla \times e^{jkr} u_k(\boldsymbol{r})\right) = \left(\frac{\omega(k)}{c}\right)^2 e^{jkr} u_k(\boldsymbol{r})$$

$$(jk + \nabla) \times \left(\frac{1}{\varepsilon(\boldsymbol{r})} (jk + \nabla)\right) \times u_k(\boldsymbol{r}) = \left(\frac{\omega(k)}{c}\right)^2 u_k(\boldsymbol{r})$$

$$\Theta_k u_k(\boldsymbol{r}) = \left(\frac{\omega(k)}{c}\right)^2 u_k(\boldsymbol{r}) \tag{2-13}$$

In this case, the new Hermitian operator is defined as:

$$(jk + \nabla) \times \left(\frac{1}{\varepsilon(\boldsymbol{r})} (jk + \nabla)\right) \tag{2-14}$$

The function "*u*", and therefore the mode profiles, is determined by the eigenvalue problem in the fourth equation of (2-13), subjected to transversality $(jk + \nabla).u_k = 0$ and the periodicity condition:

$$u_k(\boldsymbol{r}) = u_k(\boldsymbol{r} + R) \tag{2-15}$$

Because of this periodic boundary condition, eigenvalue problem can be regarded as being restricted to a single unit cell of the photonic crystal.

As *k* varies, the frequency of each band, for a given band number *n*, varies continuously. Based on that, the description of modes in photonic crystals is given as a family of

continuous functions, $\omega_n(k)$, indexed in order of increasing frequency by the band number. The information contained in these functions is called the "band structure" of the photonic crystal. Studying the band structure of a crystal provides the information that one needs to predict its electromagnetic properties. As already mentioned, a wide variety of numerical and analytical methods are available to calculate the band structure of the crystals. In the next section, "Transfer matrix method" will be studied to obtain the band structure of 1-D periodic multilayer film. Prior to that, a brief explanation around the origin of the band gap will be presented here, as the final discussion of this section.

If the dielectric constants of the materials in the periodic structure are sufficiently different, then the refractions and reflections of waves from all of the various interfaces can produce a photonic band gap. The reason is that the low frequency modes concentrate their energy in the high-ε regions, and the high frequency modes have a larger fraction of their energy in the low-ε regions

2.5 Multilayer Film

The simplest type of PBGs is one-dimensional (1-D) periodic multilayer film composed of consecutive arrangement of thin dielectric layers [1]. In this type of structures, permittivity varies periodically in space, which results in the existence of a band gap along the direction of stratification as a result of multiple reflections at the interfaces of consecutive layers. Fig.2.2 shows the schematic of 1- 2- and 3-D crystal lattices.

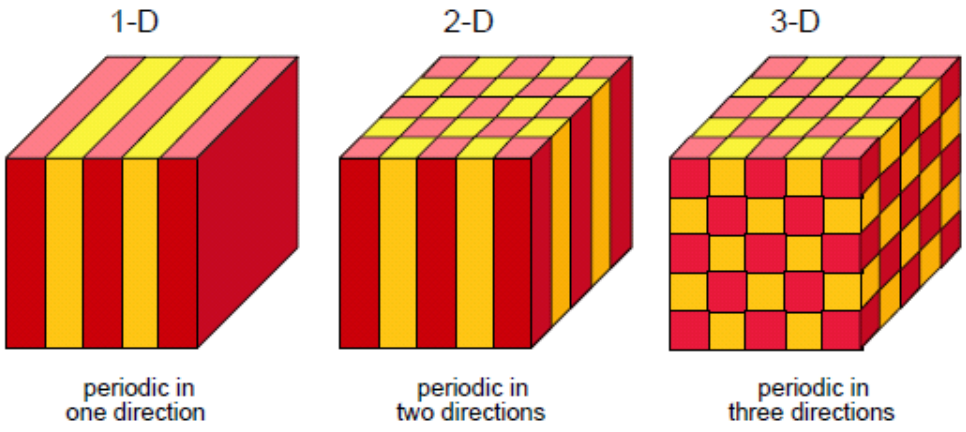

Fig.2.2Schematic of 1- 2- and 3-D crystal lattices [8]

2.5.1 Preliminary Remarks: Bragg Condition

Fig. 2.3 shows one dimensional periodic multilayer film. As this figure illustrates, one dimensional system consists of consecutive arrangement of thin dielectric layers with different electric permittivity. The system is called one dimensional because the dielectric permittivity varies only along *z* direction (direction of stratification).

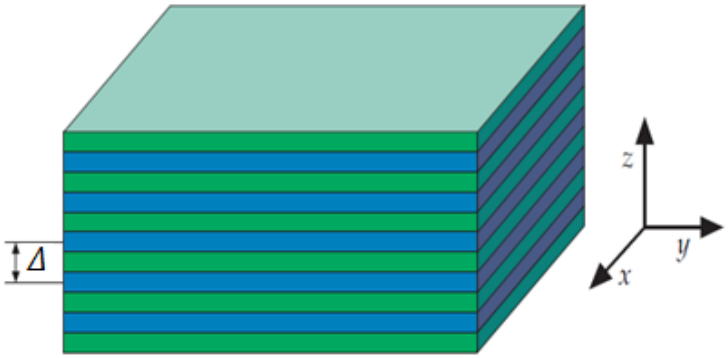

Fig.2.3 The multilayer film as a one-dimensional photonic band gap material [1].

If a plane wave is incident on the periodic layered medium, constructive or destructive interference can occur based on the angle of incidence and the spacing between layers (Δ). This problem first formulated by Sir Lawrence Bragg, is related to his work in x-ray crystallography. Based on that, constructive interference in reflection occurs when the path difference between the rays reflecting from consecutive planes are multiple of the wave length. This can be expressed through the following Bragg condition:

$$m\lambda = 2\Delta\, cos\theta \tag{2-16}$$

in which θ is the angle of incidence, $\boldsymbol{\lambda}$ the wavelength of the incident wave of the periodic medium along the stratification axis, *m* an integer number. A band gap forms when the Bragg condition (2-16) is satisfied because all reflected rays add constructively and no wave can be transmitted through the structure.

2.5.2 Wave Propagation in Periodic Layered Media: Transfer Matrix Method

Wave Propagation in periodic layered media has been studied by many researchers. Exact solution of the wave equation can be obtained in this case. An analytical investigation based on Transfer Matrix Method is proposed in [9]. The same procedure and notation are used here in order to formulate the problem.

One dimensional periodic layered medium comprised of two different materials is described with a refractive index profile as below:

$$n_{index}(z) = \begin{cases} n_2, & 0 < z < b \\ n_1, & b < z < \Delta \end{cases} \tag{2-17}$$

in which for non ferromagnetic materials the refractive indices and electric permittivity are related through: $n_1 = \sqrt{\varepsilon_1}$ and $n_2 = \sqrt{\varepsilon_2}$, and

$$n_{index}(z) = n_{index}(z + \Delta) \tag{2-18}$$

where the $\boldsymbol{z}$ axis is the direction of stratification (normal to the layer interface) and Δ is the period (same as a in previous section). The geometry of the structure is shown in Fig 2.4.

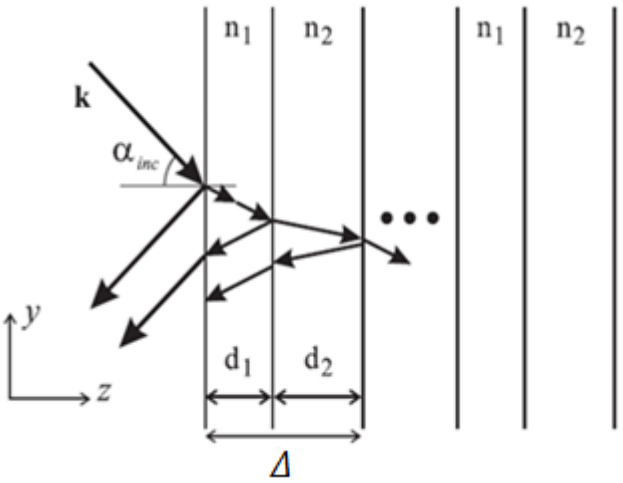

Figure 2.4: A one dimensional periodic medium. The coordinate system and light rays refracting and propagating through a stack are shown. Refractive indices of alternative regions are n_1 and n_2, respectively. Thicknesses of the regions are d_1 and d_2 [10].

The general solution of the wave equation for the multilayer structure is given in the form of Bloch waves (section 2.3):

$$\boldsymbol{E}(z)e^{j(\omega t-k_y y)} \tag{2-19}$$

where it is assumed that the plane of propagation is the ***yz*** plane. $\boldsymbol{k_y}$ is the transverse component of the wave vector. Based on Fig. 2.4, the summation of incident and reflected plane waves provide the electric field expression within each homogenous layer.

The electric field in layer $\boldsymbol{\alpha}$ ($\boldsymbol{\alpha}$=1,2) of the n^{th} unit cell is represented by a column vector in the form of:

$$\begin{pmatrix} a_n^{(\alpha)} \\ b_n^{(\alpha)} \end{pmatrix} \tag{2-20}$$

Based on that, the electric field distribution in the same layer is written as:

$$E(y,z) = \left[a_n^{(\alpha)} e^{-j(z-n\Delta)k_{\alpha z}} + b_n^{(\alpha)} e^{j(z-n\Delta)k_{\alpha z}}\right] e^{-yjk_y} \tag{2-21}$$

with

$$k_{\alpha z} = \left[\left(\frac{n_{index_\alpha}\omega}{c}\right)^2 - k_y^2\right]^{1/2} \tag{2-22}$$

Considering the continuity condition of the electric field at the interface, one can conclude that the column vectors are dependent. Consequently only one vector can be chosen arbitrarily. In the case of ***TE*** waves, applying the continuity condition for E_x and H_x ($H_x \alpha\ \partial E_x/\partial x$) at the interfaces, leads to:

$$a_{n-1} + b_{n-1} = e^{jk_{2z}\Delta} c_n + e^{-jk_{2z}\Delta} d_n$$

$$jk_{1z}(a_{n-1}+b_{n-1})=jk_{2z}(e^{jk_{2z}\Delta}c_n-e^{-jk_{2z}\Delta}d_n)$$
$$e^{jk_{2z}\Delta}c_n+e^{-jk_{2z}\Delta}d_n=e^{jk_{2z}\Delta}a_n+e^{-jk_{2z}\Delta}b_n$$
$$jk_{2z}(e^{jk_{2z}\Delta}c_n-e^{-jk_{2z}\Delta}d_n)=jk_{1z}(e^{jk_{2z}\Delta}a_n-e^{-jk_{2z}\Delta}b_n)$$

(2-23)

These four equations can be rewritten as the following two matrix equations:

$$\begin{pmatrix}1 & 1\\ 1 & -1\end{pmatrix}\begin{pmatrix}a_{n-1}\\ b_{n-1}\end{pmatrix}=\begin{pmatrix}e^{jk_{2z}\Delta} & e^{-jk_{2z}\Delta}\\ \frac{k_{2z}}{k_{1z}}e^{jk_{2z}\Delta} & -\frac{k_{2z}}{k_{1z}}e^{-jk_{2z}\Delta}\end{pmatrix}\begin{pmatrix}c_n\\ d_n\end{pmatrix}$$

(2-24)

$$\begin{pmatrix}e^{jk_{2z}a} & e^{-jk_{2z}a}\\ e^{jk_{2z}a} & -e^{-jk_{2z}a}\end{pmatrix}\begin{pmatrix}c_n\\ d_n\end{pmatrix}=\begin{pmatrix}e^{jk_{2z}a} & e^{-jk_{2z}a}\\ \frac{k_{2z}}{k_{1z}}e^{jk_{2z}a} & -\frac{k_{2z}}{k_{1z}}e^{-jk_{2z}a}\end{pmatrix}\begin{pmatrix}a_n\\ b_n\end{pmatrix}$$

(2-25)

where

$$a_n\equiv a_n^{(1)}$$
$$b_n\equiv b_n^{(1)}$$
$$c_n\equiv a_n^{(2)}$$
$$d_n\equiv b_n^{(2)}$$

(2-26)

By eliminating

$$\begin{pmatrix}c_n\\ d_n\end{pmatrix}$$

the following matrix equation is obtained:

$$\begin{pmatrix}a_{n-1}\\ b_{n-1}\end{pmatrix}=\begin{pmatrix}A & B\\ C & D\end{pmatrix}\begin{pmatrix}a_n\\ b_n\end{pmatrix}$$

(2-27)

The matrix elements are

$$A_{TE} = e^{jak_{1z}}\left[cosk_{2z}b + \frac{1}{2}j\left(\frac{k_{2z}}{k_{1z}} + \frac{k_{1z}}{k_{2z}}\right)sink_{2z}b\right]$$

$$B_{TE} = e^{-jak_{1z}}\left[\frac{1}{2}j\left(\frac{k_{2z}}{k_{1z}} - \frac{k_{1z}}{k_{2z}}\right)sink_{2z}b\right]$$

$$C_{TE} = e^{jak_{1z}}\left[-\frac{1}{2}j\left(\frac{k_{2z}}{k_{1z}} - \frac{k_{1z}}{k_{2z}}\right)sink_{2z}b\right]$$

$$D_{TE} = e^{-jak_{1z}}\left[cosk_{2z}b - \frac{1}{2}j\left(\frac{k_{2z}}{k_{1z}} + \frac{k_{1z}}{k_{2z}}\right)sink_{2z}b\right]$$

(2-28)

The complex amplitude of the plane wave in layer 1 is related to those of the equivalent layer in next unit cell through the above translation matrix. The matrix has the property of unimodularity as it relates the field amplitude of the layers that have the same refractive index. Based on that

$$AD - BC = 1$$

(2-29)

The matrix elements for ***TM*** waves are given by

$$A_{TM} = e^{jak_{1z}}\left[cosk_{2z}b + \frac{1}{2}j\left(\frac{n_2^2k_{2z}}{n_1^2k_{1z}} + \frac{n_1^2k_{1z}}{n_2^2k_{2z}}\right)sink_{2z}b\right]$$

$$B_{TM} = e^{-jak_{1z}}\left[\frac{1}{2}j\left(\frac{n_2^2k_{2z}}{n_1^2k_{1z}} - \frac{n_1^2k_{1z}}{n_2^2k_{2z}}\right)sink_{2z}b\right]$$

$$C_{TM} = e^{jak_{1z}}\left[-\frac{1}{2}j\left(\frac{n_2^2k_{2z}}{n_1^2k_{1z}} - \frac{n_1^2k_{1z}}{n_2^2k_{2z}}\right)sink_{2z}b\right]$$

$$D_{TM} = e^{-jak_{1z}}\left[cosk_{2z}b - \frac{1}{2}j\left(\frac{n_2^2k_{2z}}{n_1^2k_{1z}} - \frac{n_1^2k_{1z}}{n_2^2k_{2z}}\right)sink_{2z}b\right]$$

(2-30)

As mentioned above, just one column vector can be chosen independently.

If the column vector of layer 1 is chosen, in the zeroth unit cell, the remaining column vectors of equivalent layers are related to that the zeroth unit cell by:

$$\begin{pmatrix} a_0 \\ b_0 \end{pmatrix} = \begin{pmatrix} A & B \\ C & D \end{pmatrix}^n \begin{pmatrix} a_n \\ b_n \end{pmatrix}$$

(2-31-a)

which can be inverted to yield:

$$\begin{pmatrix} a_n \\ b_n \end{pmatrix} = \left[\begin{pmatrix} A & B \\ C & D \end{pmatrix}^{-1}\right]^n \begin{pmatrix} a_0 \\ b_0 \end{pmatrix} = \begin{pmatrix} A & B \\ C & D \end{pmatrix}^{-n} \begin{pmatrix} a_0 \\ b_0 \end{pmatrix}$$

(2-31-b)

By using the identity

$$\begin{pmatrix} A & B \\ C & D \end{pmatrix}^{-1} = \begin{pmatrix} D & -B \\ -C & A \end{pmatrix}^{-1}$$

For unimodular matrices, (2-31) can be simplified to:

$$\begin{pmatrix} a_n \\ b_n \end{pmatrix} = \begin{pmatrix} A & -B \\ -C & D \end{pmatrix}^n \begin{pmatrix} a_0 \\ b_0 \end{pmatrix}$$

(2-32)

The column vector for layer 2 of the same unit cell can always be obtained using (2-25).

2.5.3 Bloch Waves and Band Structure

Like the case of one dimensional crystal, the periodic layered media is invariant under lattice translation. Here the lattice translation operator T is defined by $T_z = z - l\Delta$, where l is an integer, it follows that:

$$T\boldsymbol{E}(z) = \boldsymbol{E}(T^{-1}z) = \boldsymbol{E}(z + l\Delta)$$

(2-33)

The transmission matrix elements derived above are a representation of the unit cell translation operator. The electric field vector of a normal mode in a periodic layered media can be written in the form of Bloch waves

$$E = E_k(z)e^{-jKz}e^{j(\omega t - k_y y)} \tag{2-34}$$

where $E_k(z)$ is periodic with period Δ, that is

$$E_K(z) = E_K(z + \Delta) \tag{2-35}$$

The subscript *K* indicates that the function $E_k(z)$ depends on *K*. Therefore, the difference between the field values at two points that are apart by an integer number of periods is the same apart from the wave propagation factor given as $e^{jkn\Delta}$.

The constant *K* is known as the Bloch wave number. So the problem is to determine *K* as function of ω and k_y.

In terms of the column vector representation, and from Eq. (2-21), the periodic condition (2-35) for the Bloch wave is:

$$\begin{pmatrix} a_n \\ b_n \end{pmatrix} = e^{-jK\Delta}\begin{pmatrix} a_{n-1} \\ b_{n-1} \end{pmatrix} \tag{2-36}$$

From Eqs. (2-27) and (2-36) it turns out that the column vector of the Bloch wave satisfies the following eigenvalue equation:

$$\begin{pmatrix} A & B \\ C & D \end{pmatrix}\begin{pmatrix} a_n \\ b_n \end{pmatrix} = e^{jK\Delta}\begin{pmatrix} a_n \\ b_n \end{pmatrix} \tag{2-37}$$

The phase factor $e^{jK\Delta}$ is thus eigenvalue of the translation matrix (A, B, C, D).

It satisfies the secular equation:

$$\begin{vmatrix} A - e^{jK\Delta} & B \\ C & D - e^{jK\Delta} \end{vmatrix} = 0$$

The solutions are:

$$e^{jK\Delta} = \frac{1}{2}(A + D) \pm \left\{ \left[\frac{1}{2}(A + D) \right]^2 - 1 \right\}^{1/2} \tag{2-38}$$

The eigenvectors corresponding to the eigenvalues are obtained from Eq. (2-37) and are:

$$\begin{pmatrix} a_0 \\ b_0 \end{pmatrix} = \begin{pmatrix} B \\ e^{jK\Delta} - A \end{pmatrix} \tag{2-39-a}$$

times any arbitrary constant. According to Eq. (2-36), the corresponding column vectors for the ***n***th unit cell are given by:

$$\begin{pmatrix} a_0 \\ b_0 \end{pmatrix} = e^{-jnK\Delta} \begin{pmatrix} B \\ e^{jK\Delta} - A \end{pmatrix} \tag{2-39-b}$$

The Bloch wave which results from Eq. (2-39) can be considered as the eigenvectors of the translation matrix with eigenvalues $e^{jK\Delta}$ given by Eq. (2-38). The two eigenvalues in (2-38) are reciprocal of each other, since the translation matrix is unimodular. Equation (2-38) gives the dispersion relation between ω, k_y and *K* for the Bloch wave function:

$$K(k_y, \omega) = \frac{1}{\Delta} cos^{-1} \left[\frac{1}{2}(A + D) \right]. \tag{2-40}$$

$\left| \frac{1}{2}(A + D) \right| < 1$corresponds to real *K* and thus to propagating Bloch waves.

When $\left|\frac{1}{2}(A+D)\right| > 1$, $= {}^{m\pi}/_{\Delta} + iK$, and so K has an imaginary part K_i and the Bloch wave is evanescent. These regions are the forbidden bands (band gaps) of the periodic medium. The band edge frequencies are those where $\left|\frac{1}{2}(A+D)\right| = 1$.

According to Eqs. (2-21) and (2-39), the final result for the Bloch wave in layer 1 of the *n*th unit cell is:

$$E_K(z)e^{-jKz} = \left[\left(a_0 e^{-jk_{1z}(z-n\Delta)} + b_0 e^{jk_{1z}(z-n\Delta)}\right)e^{jK(z-n\Delta)}\right]e^{-jKz} \tag{2-41}$$

where a_0 and b_0 are given by (2-39a). Noting that the function inside the square bracket is independent of *n*, so it is a periodic function of Δ, and is a solution of Bloch wave.

The dispersion relation (2-40) gives the Bloch wave number K along the z direction for the Bloch wave with frequency ω and y component k_y of the wave vector. The dispersion relation ω versus K for the special case $k_y = 0$ (i.e., normal incidence) is shown in Fig. 2.5. It can be written as:

$$cosK\Delta = cosk_1 a\ cosk_2 b - \frac{1}{2}\left(\frac{n_2}{n_1} + \frac{n_1}{n_2}\right) sin\ k_1 a\ sink_2 b \tag{2-42}$$

with

$$k_1 = ({}^{\omega}/_{c})n_1 \text{ and } k_2 = ({}^{\omega}/_{c})n_2 .$$

The refractive indices of the periodic layered medium are $n_1 = 1.4$ and $n_2 = 3.4$ (close to the refractive indices of SiO_2 and Si respectively) and thicknesses of the layers are $d_1 = d_2 = 0.5mm$. As Fig. 2.5 shows, the pass-bands are separated by clearly defined bandgaps. The non-zero attenuation coincides with the bandgap of the structure and reaches its maximum at the centre of the bandgap.

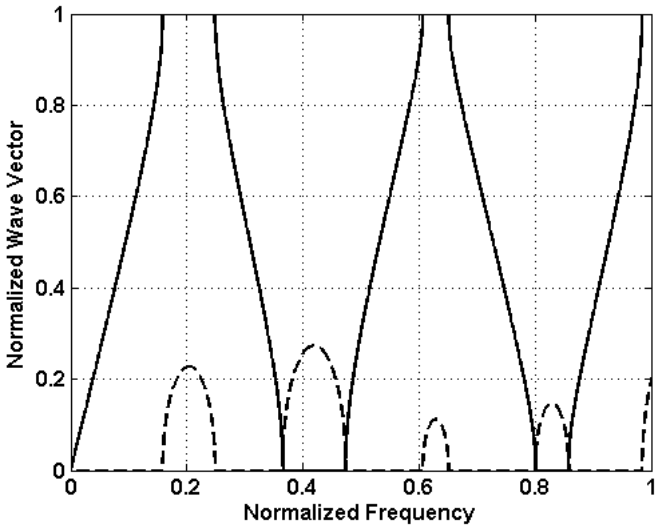

Fig.2.5: Photonic band structure of a typical one-dimensional photonic crystal for $k_y = 0$. The frequency is normalized as $^{\omega\Delta}/_{2\pi c}$ and the wave number *K* is normalized as $^{K\Delta}/_{\pi}$. The real part of the Bloch wave number (propagation constant) is shown as solid curve and its imaginary part (attenuation constant) is shown as dashed curves.

2.5.4 Microwave Circuit Analysis

As described in previous sections, the direct solution of the wave equation for the problem of multilayer film can be obtained using an analytical solution based on transfer matrix method. In this section another approach is presented for the calculation of dispersion characteristic of a multilayer film. This method relies on the calculation of scattering parameters of a single period using the full-wave software HFSS (High Frequency Simulation Software) [11] and conversion of scattering matrix to transmission matrix elements to compute the band diagram of the 1-D periodic structure.

The first step in the application of this procedure is the derivation of the equivalent network parameters for a single constituent cell of the periodic structure. This is followed by an analysis to determine the incoming and outgoing waves that propagate through the structure consisting of the cascade connection of an infinite number of the basic unit cells [12].

The relationship between the input variables V_1^+, V_1^- and the output variables V_2^+, V_2^- are found by using the $\boldsymbol{\mathcal{ABCD}}$ transmission matrix.

Figure 2.6 illustrates a two port junction with input values V_1^+, V_1^- and output quantities V_2^+, V_2^- .

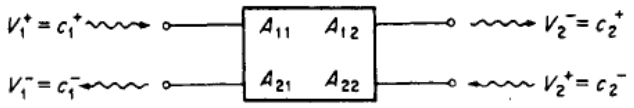

Fig.2.6. Two port network with the representation of incoming and outgoing waves [12].

The incident and reflected wave amplitudes on the input side of the junction are related to those on the output side through the wave amplitude transmission matrix. Based on Fig. 2.6, one can choose:

$$\begin{aligned} c_1^+ &= V_1^+ \\ c_1^- &= V_1^- \\ c_2^+ &= V_2^- \\ c_2^- &= V_2^+ \end{aligned} \tag{2-43}$$

The superscript + (-) refers to the amplitude of the wave propagating to the right (left).The input and output quantities are linearly related, so the matrix relation can be written as :

$$\begin{pmatrix} c_1^+ \\ c_1^- \end{pmatrix} = \begin{pmatrix} A_{11} & A_{12} \\ A_{21} & A_{22} \end{pmatrix} \begin{pmatrix} c_2^+ \\ c_2^- \end{pmatrix} \tag{2-44}$$

where the A_{nm} are frequency dependent parameters that describe the junction.

In terms of the scattering matrix for the single junction:

$$\begin{pmatrix} V_1^- \\ V_2^- \end{pmatrix} = \begin{pmatrix} c_1^- \\ c_2^+ \end{pmatrix} = \begin{pmatrix} S_{11} & S_{12} \\ S_{21} & S_{22} \end{pmatrix} \begin{pmatrix} V_1^+ \\ V_2^+ \end{pmatrix} = \begin{matrix} S_{11} & S_{12} \\ S_{21} & S_{22} \end{matrix} \begin{pmatrix} c_1^+ \\ c_2^- \end{pmatrix} \tag{2-45}$$

These equations may be solved for c_1^+ and c_1^- to give:

$$\begin{pmatrix} c_1^+ \\ c_1^- \end{pmatrix} = \begin{pmatrix} 1/S_{12} & -S_{22}/S_{12} \\ S_{11}/S_{12} & (S_{12}S_{21} - S_{11}S_{22})/S_{12} \end{pmatrix} \begin{pmatrix} c_2^+ \\ c_2^- \end{pmatrix} \tag{2-46}$$

The equations might be solved for c_1^- and c_2^+ in terms of c_1^+ and c_2^- to give:

$$\begin{pmatrix} c_1^- \\ c_2^+ \end{pmatrix} = \begin{pmatrix} A_{21}/A_{11} & (A_{11}A_{22} - A_{12}A_{21})/A_{11} \\ 1/A_{11} & (-A_{12})/A_{11} \end{pmatrix} \begin{pmatrix} c_1^+ \\ c_2^- \end{pmatrix} \tag{2-47}$$

These two set of formula relates S parameters to transmission matrix parameters and vice versa. Once the Scattering parameters are obtained either analytically or numerically, the transmission matrix elements can be obtained using the conversion relation (2-46), and then dispersion diagram can be obtained using (2-40).

2.5.5 Transmission Matrix Elements and Band Structure of Stratified Medium: Revisited

In order to verify the validity of the method proposed in previous section, 1-D multilayer film structure composed of consecutive arrangement of thin dielectric layers will be investigated in this section.

The geometry of the cell element of the proposed 1-D PBG structure composed of consecutive arrangement of thin dielectric layers, are shown in Fig. 2.7. The thickness of the single period is D and it consists of two dielectrics layers with thicknesses equal to $d_1 = d_2 = 0.5mm$ and refractive indices equal to $n_1 = 1.4$ and $n_2 = 3.4$,respectively (same as structural parameters for the results shown in Fig. 2.5). The width and length of the cross section of the structure are $a = b = 5mm$.

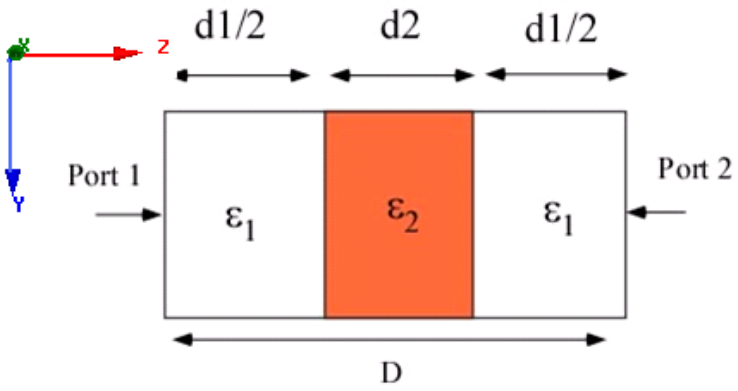

Fig.2.7: Geometry of the multilayer film structure

To calculate dispersion characteristic of the 1-D multilayer film, scattering parameters of a single layer of the structure are calculated using HFSS [11]. Master and slave boundary conditions along with Floquete port excitation are used to capture the periodic lattice of a single layer and plane wave excitation. Transmission matrix elements of the single layer are then obtained from the knowledge of the scattering matrix of that same single layer. Then, dispersion characteristic of the 1-D PBG structure is derived using transmission matrix of a single layer using dispersion relation (2-40).

The dispersion curve obtained by the conversion method is shown in Fig 2.8. In this figure, the solid curve represents the dispersion diagram obtained through transfer matrix method, while the dashed curve represents the same obtained through the conversion technique and HFSS. As this figure shows, there is good agreement between the results of the analytical method and our numerical results. It is to be noted that normalized frequency and wave vector have been used in this plot.

In order to validate the implementation of the multilayer structure in HFSS and the conversion routines developed in MATLAB, the structure shown in Fig. 2.7 was characterized using a cascade of analytical expressions for the transfer matrix (T) as well as through HFSS simulations. Fig. 2.9 shows the results of these calculations which demonstrate excellent agreement between the two methods.

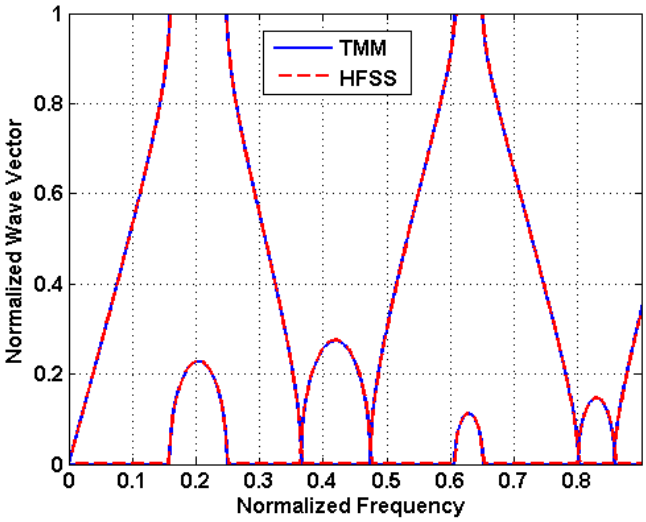

Fig.2.8: Photonic band structure of a typical one dimensional photonic crystal for $k_y = 0$. The frequency is normalized as $\omega\Delta/2\pi c$ and the wave number K is normalized as $K\Delta/\pi$.

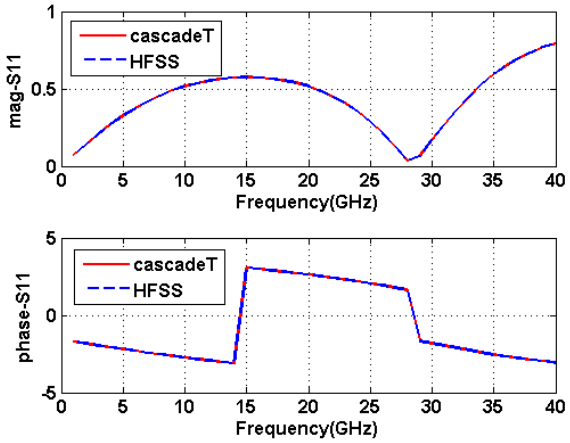

(a)

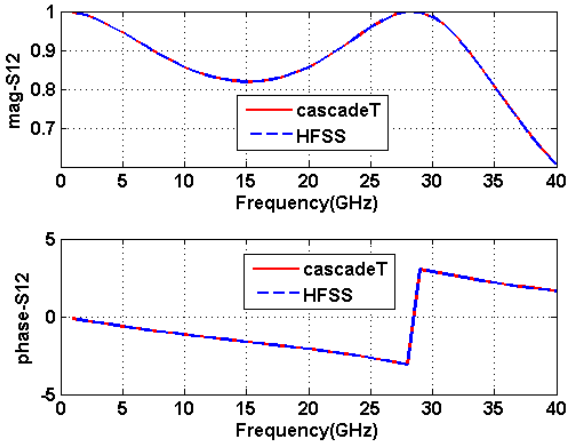

(b)

Fig.2.9: S parameters for cascading of 2 layers of Fig. 2.7, obtained by HFSS simulation and multiplying T matrices (a) S11 (b) S12. Phase is in radian.

2.6 Conclusion

In this chapter, the dispersion characteristic of 1-D multilayer film was determined using an analytical method based on the transfer matrix technique.

An approach based on scattering matrix to transmission matrix elements conversion was proposed to obtain the dispersion characteristics of 1-D multilayer film. In this approach, scattering parameters of a single layer of the structure were calculated using commercial software HFSS. The transmission matrix of single layer is then obtained from the knowledge of its scattering matrix. Then, the dispersion characteristic of a 1-D PBG structure is derived using the transmission matrix of a single layer.

In the coming chapters of this work, S-parameters of single period of 1-D photonic band gap structures composed of inclusions (*i.e.* dipole element or SRR) will be calculated using HFSS and the dispersion characteristic obtained by the method proposed in this chapter.

2.7 References for Chapter 2

1. J.D. Joannopoulos, S.G. Johnson, J.N. Winn, and R.D. Meade, *Photonic Crystals Molding the Flow of Light*, Princeton University Press, Princeton, 2008.
2. K. Sakoda, *Optical Properties of Photonic Crystals*, Springer, Berlin, 2001.
3. P. Yeh, *Optical Waves in Layered Media*, Wiley, New-York, 1988.
4. C. Kittel, *Introduction to Solid State Physics*, Wiley, New-York, 1996.
5. J. Mathews and R. Walker, *Mathematical Methods of Physics*, Addison-Wesley, Redwood-City, 1964.
6. D.N. Chigrin, A.V. Lavrinenko, D.A. Yarotsky, and S.V. Gaponenko, "All-dielectric one-dimensional periodic structures for total omnidirectional reflection and partial spontaneous emission control," *J. Lightwave Tech*., vol. 17, pp. 2018-2024, 1999.
7. D.N. Chigrin, and C.M. Sotomayor Torres, "Periodic thin-film interference filters as one-dimensional photonic crystals," *Opt. Spectrosc*., pp. 1-6, 2001.
8. http://ab-initio.mit.edu/photons/tutorial/photonic-intro.pdf, accessed June 2012.
9. A. Yariv and P. Yeh, *Electromagnetic Propagation in Periodic Media, in Optical Waves in Crystals: Propagation and Control of Laser Radiation*, Wiley, Hoboken, 2003.
10. D. N. Chigrin, "Electromagnetic wave propagation in photonic crystals with incomplete photonic band gap", PhD Thesis, 2003
11. HFSS ver. ver. 12. Pittsburgh, PA, Ansoft Corp.
12. R.E. Collin, "Chapter 8: Periodic Structures and Filters," *in Foundations for Microwave Engineering*, 2nd Ed. IEEE Press, New-York, 1991.

Chapter 3

Dispersion Characteristics of 1-D PBG Structures Composed of Subwavelength Dipole Elements

3.1 Introduction

As discussed in previous chapters, the simplest type of PBGs is one dimensional periodic multilayer film. The properties of stop-band and pass-band of such structures have been broadly investigated in previous sections.

The other type of 1-D photonic band gap materials, which is the subject of this chapter, is a cascade connection of layers that are comprised of inclusions (*i.e* dipoles) imbedded within a host medium [1]. Multiple reflection between consecutive layers results in Bragg diffraction phenomenon which leads to the emergence of band gap in such structures. Frequency band and width of the band gap can be adjusted by modifying scattering parameter of each constituent layer.

Further investigation of such artificial media shows that judicious selection of design parameters of the cell element can lead to a certain response in terms of the polarization, frequency and propagating angle of the mode. Therefore, the proposed 1-D PBG structures that are studied in this chapter can be used as frequency and polarization selective structures [2].

The analytical method that is used in this chapter, relies on the calculation of scattering parameters of a single layer using the full-wave software HFSS (High Frequency Simulation Software) [3] and conversion of scattering matrix to transmission matrix elements to compute the band diagram of the 1-D periodic structure [4,5], as discussed and verified in previous chapter. As the scattering parameters describe reflection and transmission properties of this structure, high reflection and high transmission windows are representatives of the stop-band and the pass-band of the structure, respectively, and will be shown to be in agreement with dispersion characteristic of the 1-D PBG structure.

In this chapter, we first investigated suspended membrane structures that are surrounded entirely by air (free standing case). Then we generalized this study to cover the case where the dielectric substrate is used as the host material.

3.2 Theory

The 3-D geometry of the cell element and top views of 1-D PBG structure composed of layers of Perfect Electric Conductor (PEC) dipoles are shown in Fig. 3.1. The layers are *D* apart along the longitudinal *z*-axis and T_x and T_y are lattice dimensions in the transverse *xoy* plane. The length and width of the dipole are represented by *l* and *w*, respectively. To obtain the dispersion characteristic of the 1-D PBG structure, scattering parameters of a single layer of dipoles are calculated using HFSS [3]. Master and slave boundary conditions along with Floquete port excitation is used to capture the periodic lattice of a single layer and plane wave excitation. It is assumed that the separation between layers is large enough to avoid coupling through higher order Floquete modes. Transmission matrix elements of the single layer are then obtained from the knowledge of the scattering matrix of that same single layer. Then, dispersion characteristic of the 1-D PBG structure is derived using transmission matrix of a single layer as described below. The relationship between scattering matrix and transmission matrix elements was derived in the previous chapter and is given in the following for the sake of completeness:

$$\begin{pmatrix} c_1^+ \\ c_1^- \end{pmatrix} = \begin{pmatrix} 1/S_{12} & -S_{22}/S_{12} \\ S_{11}/S_{12} & (S_{12}S_{21} - S_{11}S_{22})/S_{12} \end{pmatrix} \begin{pmatrix} c_2^+ \\ c_2^- \end{pmatrix} \tag{3-1}$$

where the subscript in vector elements represents the port number and the superscript refers to incident (positive for incoming) or reflected (negative for outgoing) waves. The dispersion relation can be obtained using the transmission matrix elements of a single layer [7]:

$$K(k_t, \omega) = \frac{1}{D} cos^{-1}\left[\frac{1}{2}(A_{11} + A_{22})\right] \tag{3-2}$$

in which *"D"* represents the longitudinal periodicity of 1-D PBG lattice shown in Fig. 3.1a, k_t is the transverse component of the wave vector and ω the angular frequency. A_{11} and A_{22} are the transmission matrix elements of a single cell.

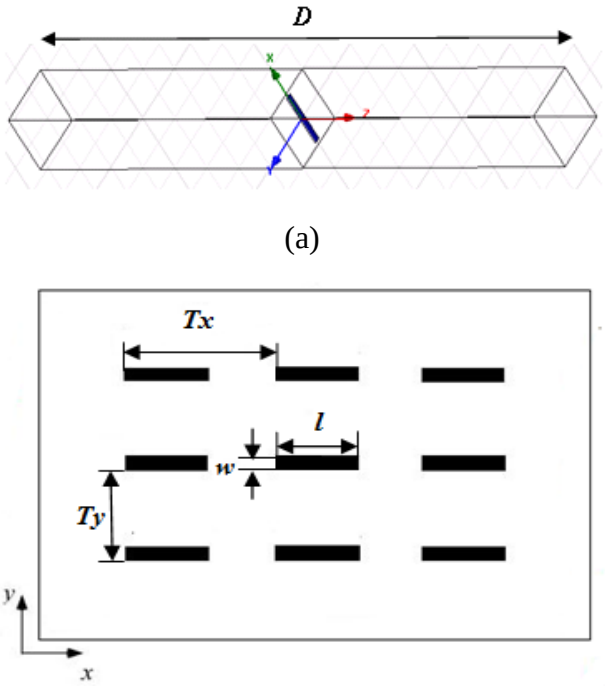

Fig. 3.1. (a) Three dimensional geometry of single cell of the PBG structure. (b) Top view of the PBG structure in the transverse *xoy* plane. The notation shown in this figure for the geometrical parameters will be used throughout this chapter. The same structure shown in (b) is repeated along *z* axis with period *D*.

3.3 Dispersion characteristic as function of cell element configuration

Numerous simulations were carried out to investigate the effect of the geometrical parameters of the conductive elements (*e.g.* dipoles) on the dispersion characteristic of the 1-D PBG structure. In this chapter, the excitation is assumed to be normal incident plane wave (wavevector parallel to z-axis) with E-field parallel to dipole unless otherwise noted. The geometrical parameters for a unit cell of the structure in first set of simulations are described in Table 3.1.

The separation between the two consecutive layers was set at *D*=20.0 mm. As seen, the dipole width was kept constant while its length was changed and the lattice size along the dipole length was changed simultaneously to accommodate the cell element.

The simulation results for scattering parameters of a single layer of the PBG structure are shown in Fig. 3.2. It can be seen that the reflection (transmission) coefficient increases (decreases) as the length of the dipole is increased. Therefore, wider bandgap is expected for PBG structures with constituent layers of higher reflectivity. This is in agreement with the phenomenon that is observed in the case of stratified 1-D dielectric PBG structure which demonstrates wider bandgap as the level of multiple reflections between layers is increased by raising permittivity contrast between layers [8].

Table 3.1: Geometrical parameters for dipole structure shown in Fig. 3.1.

Structure	T_x	T_y	l	w
Str1	1mm	0.4mm	0.9mm	0.1mm
Str2	2mm	0.4mm	1.8mm	0.1mm
Str3	3mm	0.4mm	2.8mm	0.1mm

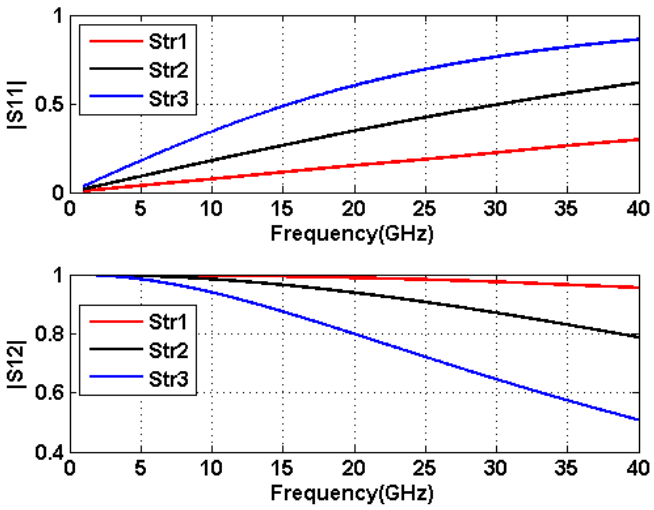

Fig. 3.2. S-parameters of the single layer of the structures described in Table 3.1.

As mentioned, the dispersion characteristics of the three structures listed in Table 3.1 were obtained from the knowledge of the scattering parameters of a single constituent layer of the PBG (Fig. 3.3). Note that normalization factors for propagation and attenuation constants are assumed to be D/π throughout this chapter.

The normalized propagation constant is plotted in Fig. 3.3-a, showing that a wider band gap can be achieved by increasing the dipole length (for the same dipole width). Figure 3.3-b shows the normalized attenuation constant for the same set of structures. The non-zero attenuation coincides with the bandgap of the structure and reaches its maximum at the centre of the bandgap which is generally the case for 1-D PBG structures. Transmission through 1-D finite PBG structure composed of 15 layers of dipoles was then calculated using the T-matrix cascade method [7,9] and the results shown in Fig. 3.4. It can be seen that "no-transmission" regions match the bandgap region of the respective structure and this is consistent with the dispersion calculations presented in Fig. 3.3.

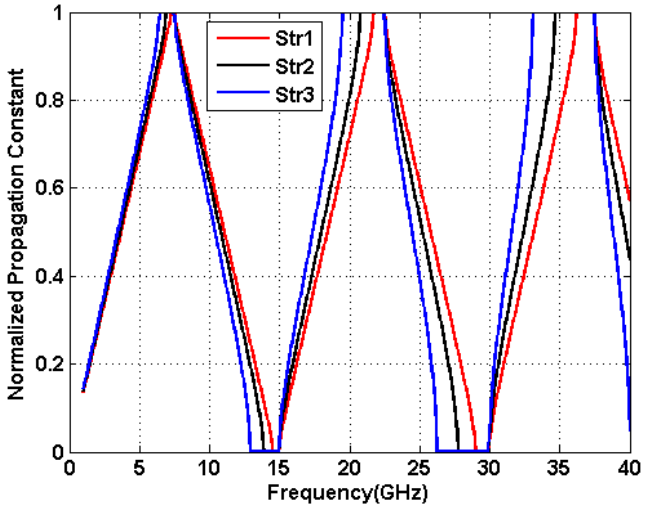

(a)

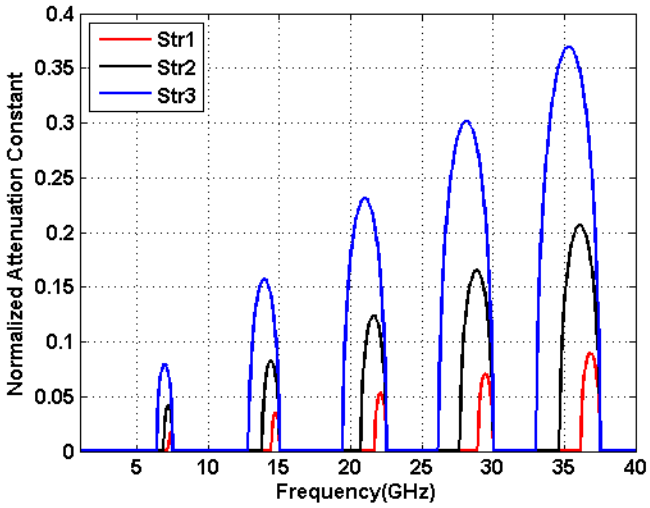

(b)

Fig. 3.3.(a). Normalized propagation constant (b) Normalized attenuation constant. The legend refers to the structures described in Table 3.1.

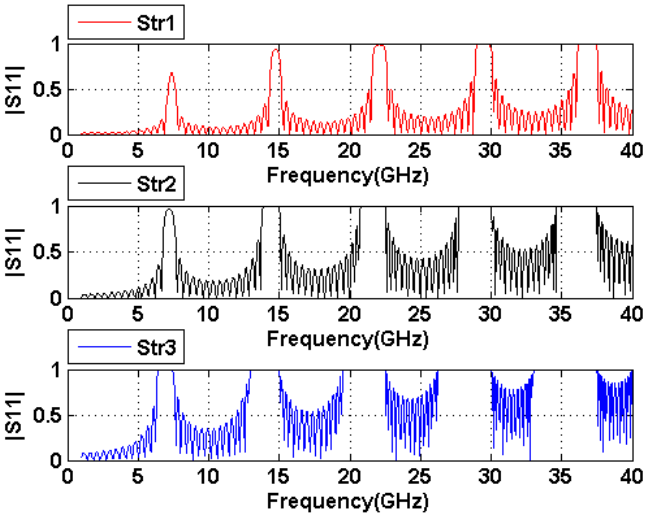

(a)

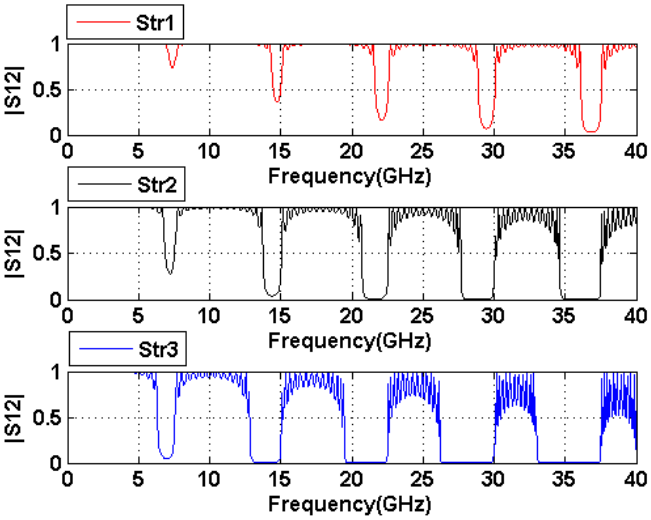

(b)

Fig. 3.4. Scattering response of the cascade of 15 layers of structures listed in Table 3.1: (a) Reflectance (b) Transmittance.

Another set of simulations was performed to examine the effect of the periodicity D on the dispersion characteristics of 1-D PBG structures. In this set of simulations, the lattice parameters were T_x=1mm, T_y=0.4mm, and the dipole parameters were l=0.9mm and w=0.1mm. The simulations were performed for three different value of D and the results are shown in Fig. 3.5. Based on these results, one can observe that by increasing the separation between the consecutive layers (D), the number of stop-band and pass-bands will increase. Also, the larger the separation, the smaller the size of the bandgap.

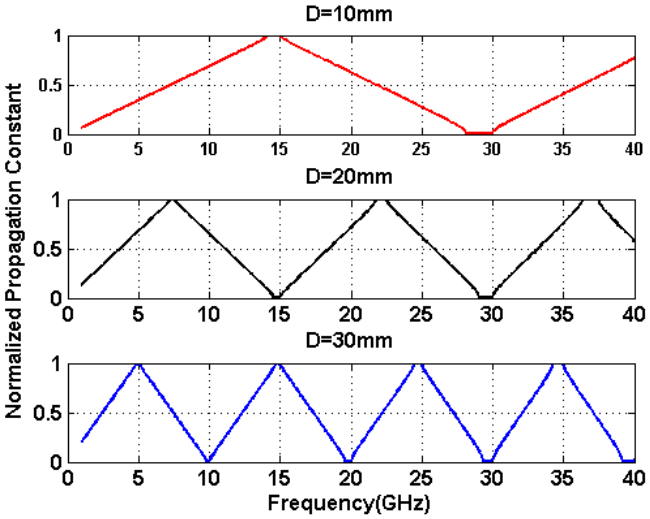

Fig. 3.5. Dispersion curve for three different separations between the consecutive layers (D).

Another factor that provides a degree of control over the bandgap, is the cell geometry. In order to examine the effect of this parameter, simulations were performed for a number of cases with different T_y while all other parameters were kept constant as follows: D=10.0mm, T_x=1mm, l=0.9mm and w=0.1mm. It is assumed that the dipole runs parallel to the x-axis. The simulation was performed for two different lattice widths of T_y=0.4mm and T_y=1.0mm and the results are shown in Fig. 3.6. It can be observed that diminishing T_y size results in wider bandgap, while the location of the bandgap remains intact.

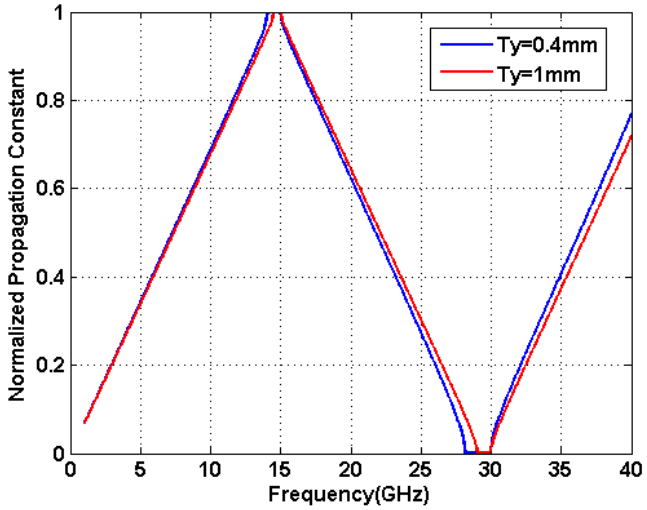

Fig. 3.6. Dispersion curve for two different lattice widths.

3.4 Angular sensitivity

A set of simulations was carried out in order to investigate the variation of dispersion characteristics for the two TM and TE polarizations as the propagating angle of modes is changed (*xoy* is defined as the transverse plane). For TE (TM) polarization, it is assumed that *E* (*H*) field polarization is parallel (normal) to the dipole length. The angle of propagation through the structure was defined as the angle of wavevector of the given mode of the 1-D crystal with respect to the longitudinal *z*-axis. In this set of simulations, the periodicity of the structure is D=10.0mm. The lattice parameters are T_x=T_y=1mm, l=0.9mm, and w=0.1mm.The angle of propagation was changed from 10^o to 60^o and the transverse component, k_t, varied accordingly to calculate the dispersion characteristic using Eq. (3.2).

Figure 3.7-a shows the dispersion curve for the structure in Fig. 3.1 for TM polarization. As this figure shows, the gap shifts by increasing the angle of propagation while the size of the gap remains relatively constant for TM incidence. Also, it is worth noting that the second gap is wider than the first one. Figure3.7-b shows the simulation results for the TE case. It demonstrates that the gap shifts as the angle of propagation is increased and also the size of the gap increases significantly as opposed to TM polarization. Again in this case, the second gap is wider than the first one.

The projected band diagram, for an infinite cascade of layers composed of dipole elements is depicted in Fig. 3.8. In this diagram the transverse component of the wave vector (k_t), is calculated through:

$$k_t = \frac{\omega}{c}\sin\alpha \tag{3-3}$$

where α is the angle of propagation with respect to the *z*-axis and ω is the angular frequency. The angular response of the structure can be summarized in the projected band diagram shown in Fig. 3.8 for TM (right panel) and TE (left panel) polarizations. The normalization factor of the transverse component of the wave vector is D/π. In this figure, 9. A plane wave with operating frequency and k_t in the white region of Fig. 3.8 cannot propagate through the 1-D PBG structure and will be reflected back. These high reflection areas are strongly dependent on the angle of propagation and the frequency. It is interesting to note that the

bandgap shifts to higher frequencies for both polarizations as the angle of propagation is increased.

What is observed in the case of 1-D PBG comprised of dipoles is in agreement with the observation made in the case of a stratified dielectric medium, in which the size of the gap increases for the first two bands in TE polarization as k_t is increased. The only difference between the two cases is that in the case of stratified dielectric medium, TM bandgaps shrink to zero when the angle of propagation coincides with Brewster angle, while there is no such phenomenon in the case of PBG structures comprised of dipole layers [7].

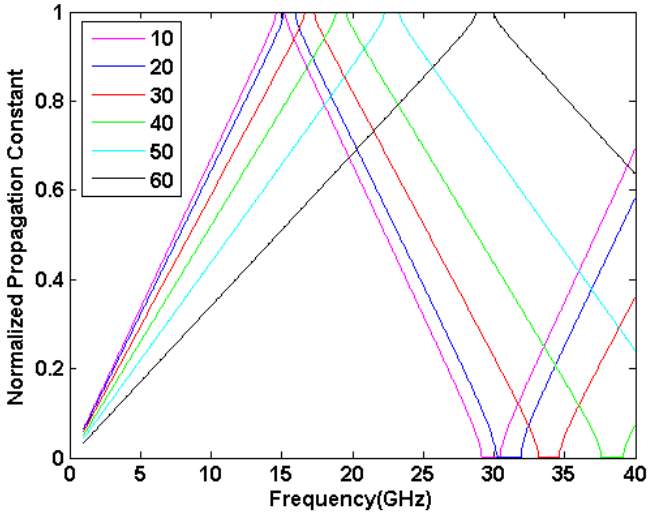

(a)

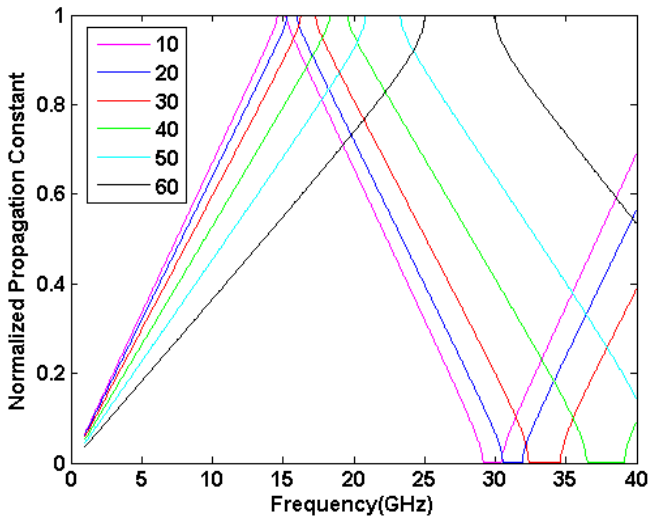

(b)

Fig. 3.7. Dispersion curves for different angle of propagations for the structure shown in Fig. 3.1 (a) TM Polarization, (b) TE polarization.

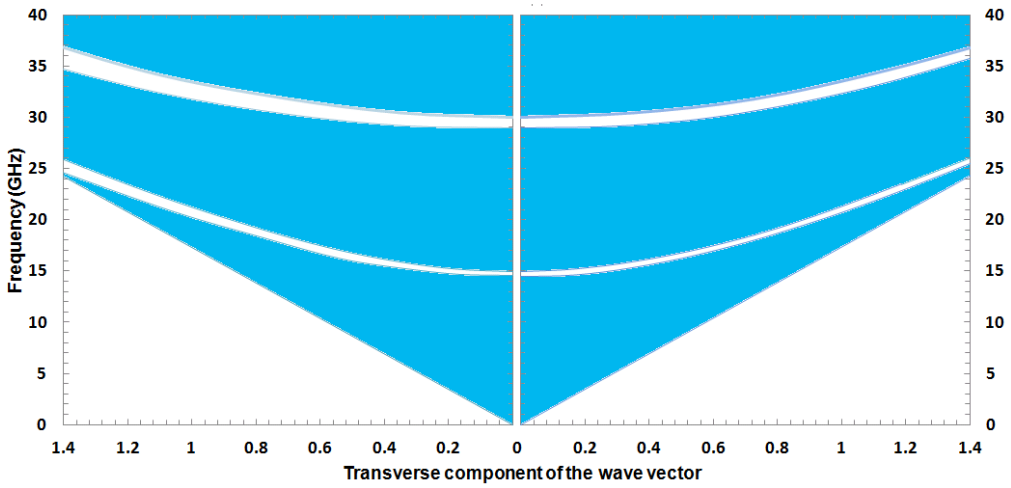

Fig. 3.8. Projected Band Diagram for the structure shown in Fig. 3.1 for TM polarization (right panel) and TE polarization (left panel).

3.5 Simultaneous Polarization and Frequency Selectivity

The idea of interlacing dipoles to achieve a novel PBG with simultaneous polarization and frequency selectivity is investigated in this section. To achieve this, a set of simulations were carried out for propagating mode along the *z* axis, with *E*-field polarization being either parallel or normal to the dipole. Figure 3.9 illustrates the dispersion curve for the structure described in Fig. 3.1 for D=10.0mm, T_x=T_y=1mm, l=0.9mm, and w=0.1mm. It can be seen from Fig. 3.9 that for the *E*-field polarization parallel to dipole, interaction occurs between the excitation and the structure that results in the emergence of bandgap. While for the other polarization (*E*-field normal to dipole), there is no interaction between dipole elements and the incident field and, as a result, the incoming wave passes through without any obstruction from the 1-D PBG structure. This observation suggests the possibility of interlacing dipoles of orthogonal orientation within the same 1-D PBG structure to independently control the bandgap behaviour for two orthogonal polarizations. A single period of the proposed structure is shown in Fig. 3.10. It is composed of two different layers of dipoles namely, layers *A* and layer *B* with *z* axis periodicities of D_A and D_B, respectively. Also, it should be noted that the orientation of dipoles on layer *A* are orthogonal to the orientation of dipoles on layer *B*. The same geometrical parameters T_x=T_y=1mm, l=0.9mm, and w=0.1mm were used for the dipoles on both layers while D_A=10.0mm and D_B=5mm.

Figure 3.11 shows dispersion characteristic for a normally propagating plane wave when the *E*-field polarization is parallel to dipoles on layer *A*. The dispersion characteristic shown in Fig. 3.11 demonstrates the existence of two separate bandgaps around 15GHz and 30GHz.

The solid curve in this figure represents the dispersion diagram when only layer *A* is present, while the dashed curve represents the same when both layers *A* and *B* are present. It can be concluded that for modes with *E*-field polarization parallel to dipoles on layer *A*, the locations of stop-band and pass-band are not affected by the presence of layer *B*.

Subsequently, simulations were carried out to study the effect of polarization parallel to the dipoles on layer *B* and the results are shown in Fig. 3.12. There is only one band gap around 30 GHz within the simulated frequency band and the bandgap turns out to be wider than the bandgap of the dispersion characteristic shown in Fig. 3.11 around this same frequency. There is no bandgap around 15GHz as opposed to what was observed in Fig. 3.11 for *E*-field polarization parallel to dipoles on layer *A*. Again, the location of stop-band and pass-band do not change by removing layer *A* when *E*-field polarization of the mode is parallel to dipoles on layer *B*. Figures 3.11 and 3.12 show clearly that it is practical to independently modify the bandgap behaviour of the two orthogonal polarizations. In order to further substantiate this statement, the possibility of widening the bandgap for one of the two polarizations was studied through adjustment of the layer with dipoles parallel to that same polarization. The proposed structure is shown in Fig. 3.13. Relative location of layers *A* and *B* are the same as described in Fig. 3.10. However, the lattice size of the dipoles on layer *A* has been reduced in order to widen the lower bandgap around 15GHz.

Dispersion characteristic of this structure is shown in Fig. 3.14 which demonstrates the presence of bandgaps around 15GHz and 30GHz for the modal polarization parallel to dipoles on layer *A*. It can be seen that the width of the lower (upper) bandgap has increased to 2.1GHz (1GHz) as compared to the dispersion characteristic shown in Fig. 3.11. The dispersion curve is the same with and without layer *B* which demonstrates that the dispersion characteristic of the structure is insensitive to the presence of layer *B* when the polarization of the modal *E*-field is parallel to dipoles on layer *A*. This example shows the possibility of controlling the width of the bandgap for a given polarization without altering dispersion characteristic for the other polarization.

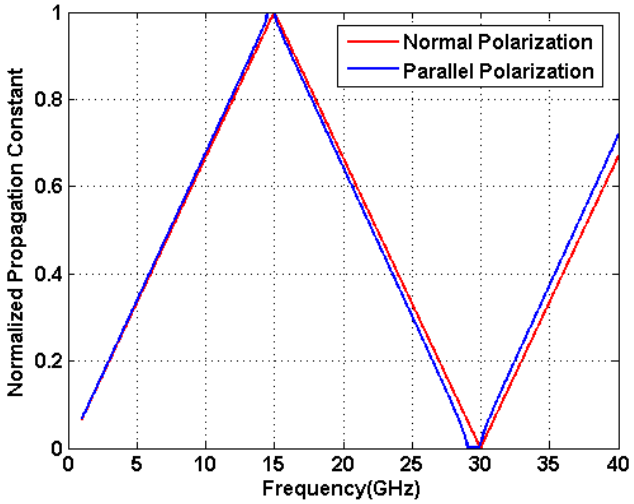

Fig. 3.9. Dispersion characteristic of the structure shown in Fig. 3.1 when T_x=1mm, T_y=1mm, l=0.9mm, and w=0.1mm for normal propagating mode with the E-field parallel or normal to the dipole.

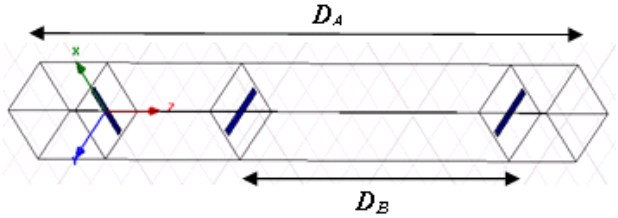

Fig. 3.10. Three dimensional geometry of single cell of PBG structure composed of cascade connection of dipoles with orthogonal orientation.

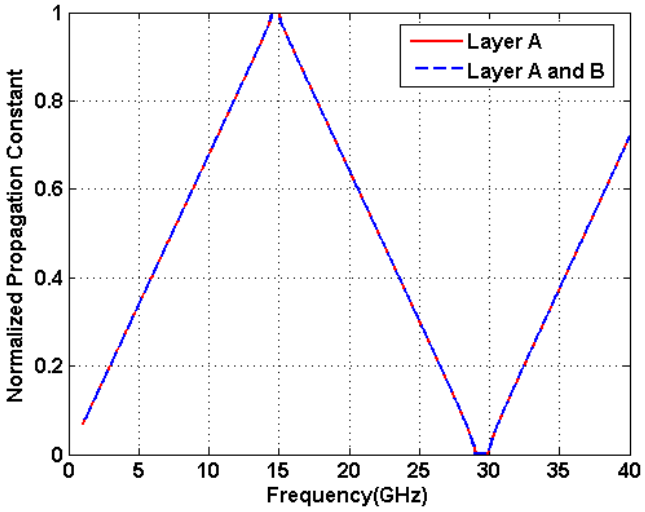

Fig. 3.11. Dispersion curve for the structure of Fig. 3.10 for normal propagating modes with E-field polarization parallel to dipoles on layer A. The solid curve in this figure represents the case that just layer *A* is present in Fig. 3.10, while the dashed curve represents the case that both layers *A* and *B* are present.

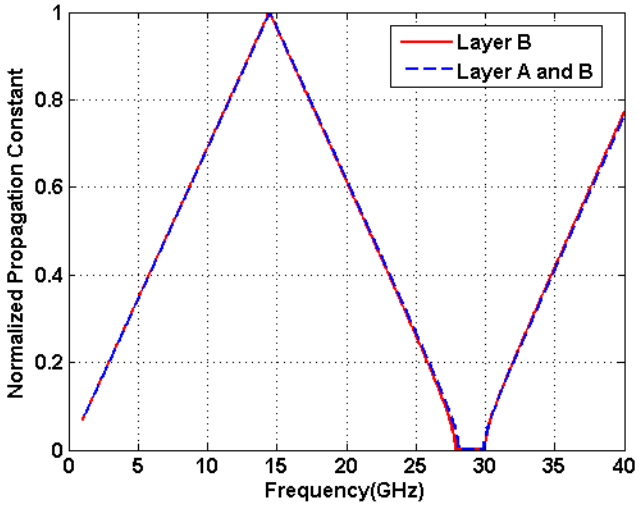

Fig. 3.12. Dispersion curve for the structure of Fig. 3.10 for normal propagating modes with E-field polarization parallel to dipoles on layer B. The solid curve in this figure illustrates the case that just layer *B* is present in Fig. 3.10, while the dashed curve represents the case that both layers *A* and *B* are present.

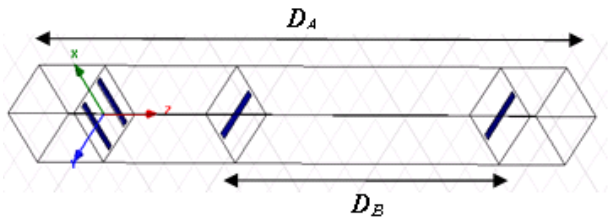

Fig. 3.13. Three dimensional geometry of single cell of PBG structure composed of cascade connection of dipoles with orthogonal orientation.

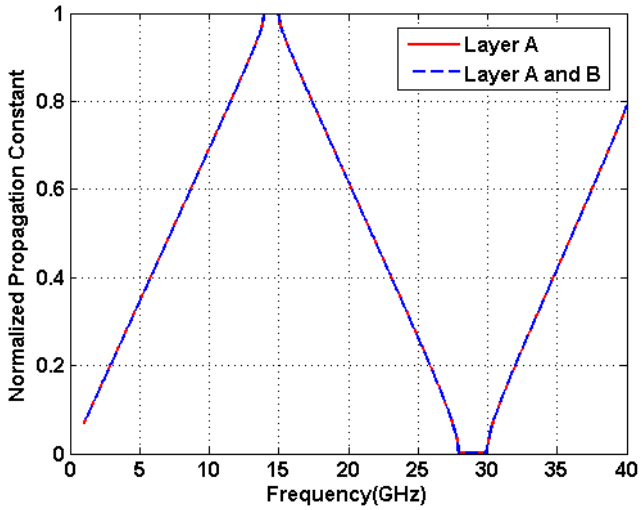

Fig. 3.14 Dispersion curve for the structure of Fig. 3.13 when modal polarization matches the dipoles on layer A. The solid curve in this figure illustrates the case that just layer *A* is present in Fig 3.13, while the dashed curve represents the case that both layers *A* and *B* are present

The same procedure was repeated for modal polarization parallel to dipole on layer *B*, and the results are shown in Fig. 3.15. The solid curve in this figure represents the dispersion diagram when only layer *B* is present, while the dashed curve represents the same when both layers *A* and *B* are present. Again, close agreement between the two dispersion curves demonstrates that the presence of layer *A* does not modify the dispersion characteristic of the structure when modal polarization is parallel to dipoles on layer *B*.

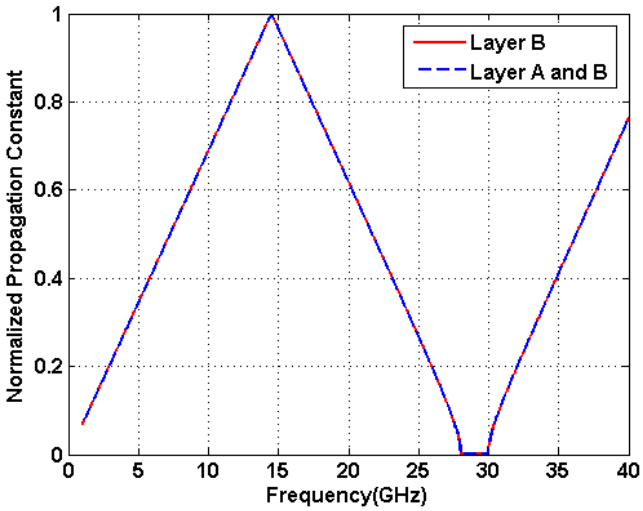

Fig. 3.15: Dispersion curve for the structure of Fig. 3.13 when modal polarization matches the dipoles on layer B. The solid curve in this figure illustrates the case that just layer *B* is present in Fig 3.13, while the dashed curve represents the case that both layers *A* and *B* are present.

3.6 Effect of Substrate

To understand the effect of the presence of substrate on the dispersion characteristic of the 1-D PBG structure, a set of simulation was performed for propagating mode along *z* axis and polarization of the *E*-field being either parallel or normal to the dipole. In this set of simulations, the lattice parameters were T_x=T_y=1mm, and the dipole parameters were *l*=0.9mm and *w*=0.1mm. Substrate thickness is equal to *h*=0.5mm and its electric permittivity isε=3 (Rogers RO3003). The simulations were performed for three different values of *D* and the results are shown in Fig. 3.16. Based on this result, one can observe that by increasing the separation between the consecutive layers (*D*), the number of stop-bands and pass-bands will increase. Also, it can be observed that, the bandgap is wider for parallel polarization rather than normal polarization, because of the fact that, for *E*-field polarization parallel to dipole,

interaction occurs between the excitation and the dipole that results in the emergence of bandgap. On the other side, for the other polarization (*E*-field normal to dipole), there is no interaction between dipole elements and the incident field, but the presence of the substrate leads to the emergence of bandgap.

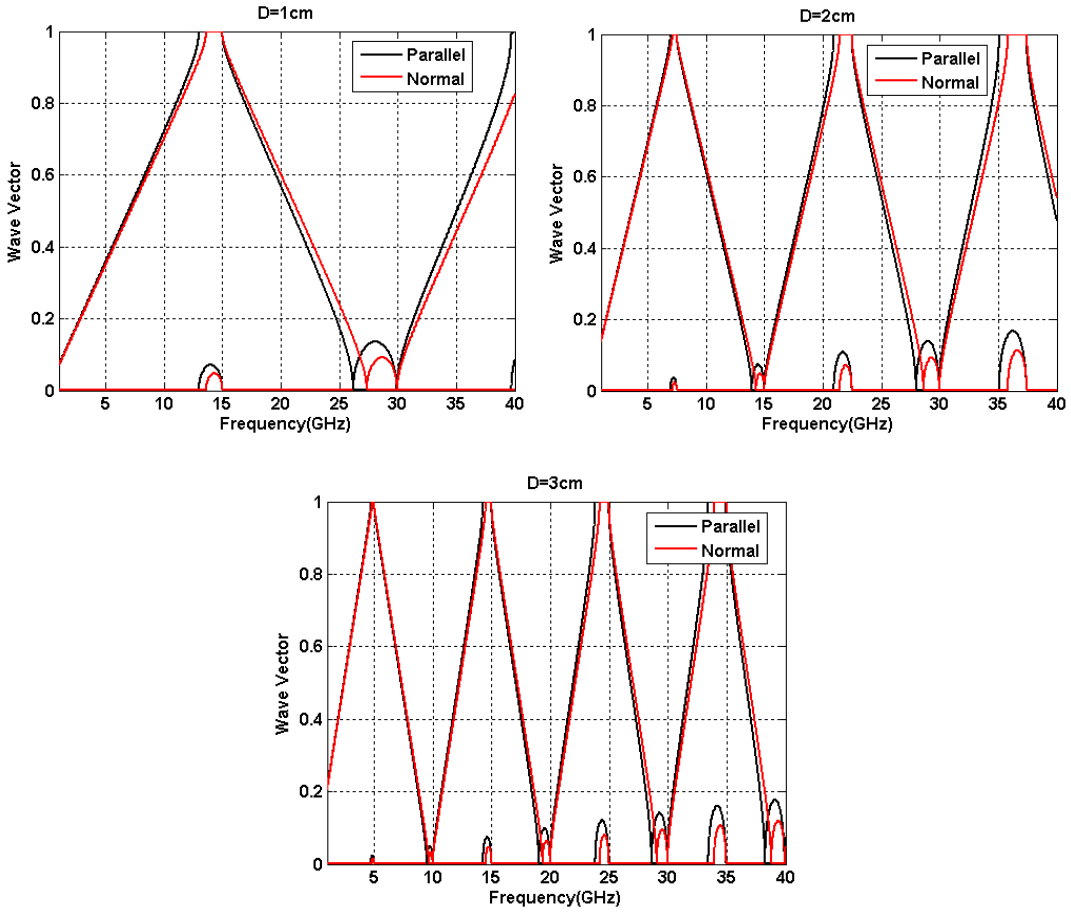

Figure 3.16: Dispersion curve for three different separations between the consecutive layers (*D*) for E field polarization parallel or normal to the dipole.

In order to verify the above statement, a set of simulations was performed to compare the results of bare substrate and polarization of incident field normal to the dipole. The simulation parameters are identical to those in the previous case. As shown in Fig. 3.17, there is a close agreement between dispersion characteristics of these two cases, leading to the conclusion that in the case of polarization normal to the dipole length, the band gap is merely caused by substrate.

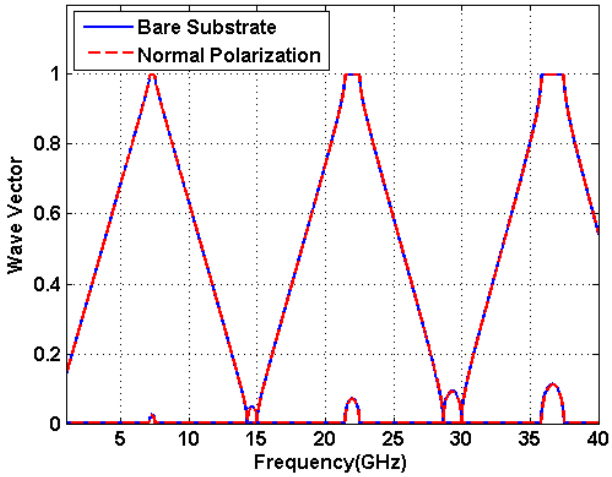

Fig. 3.17: Dispersion curve for normal polarization and bare substrate case.

In order to investigate the polarization sensitivity of the structure, while the substrate is present, the same procedure described in section 3.5 is repeated. The proposed structure, shown in Fig. 3.18, is the same as the structure shown in Fig. 3.10. The only difference is the presence of substrate. The same geometrical parameters of T_x=T_y=1mm, l=0.9mm, and w=0.1mm were used for the dipoles on both layers while D_A=10.0mmand D_B=5mm.Substrate thickness was set to h=0.5mm and its relative permittivity set to 3 (Rogers RO3003).

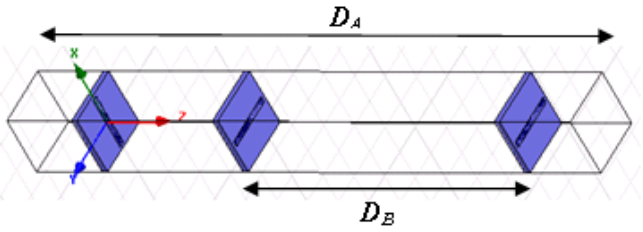

Fig. 3.18. Three dimensional representation of a single cell of PBG structure composed of cascade connection of dipoles with orthogonal orientation. The substrate is present in this case.

Figure 3.19 shows the dispersion characteristic for normally propagating plane wave when the *E*-field polarization is parallel to dipoles on layer *A*. The dispersion characteristic shown in Fig. 3.19 demonstrates the existence of two separate bandgaps around 15GHz and 30GHz. The solid curve in this figure represents the dispersion diagram when only layer *A* is present while the dashed curve represents the same when both layers *A* and *B* are present. It can be concluded that for modes with E-field polarization parallel to dipoles on layer *A*, the widths

of stop-band and pass-band of the structure are affected by the presence of layer *B*, while substrate is present.

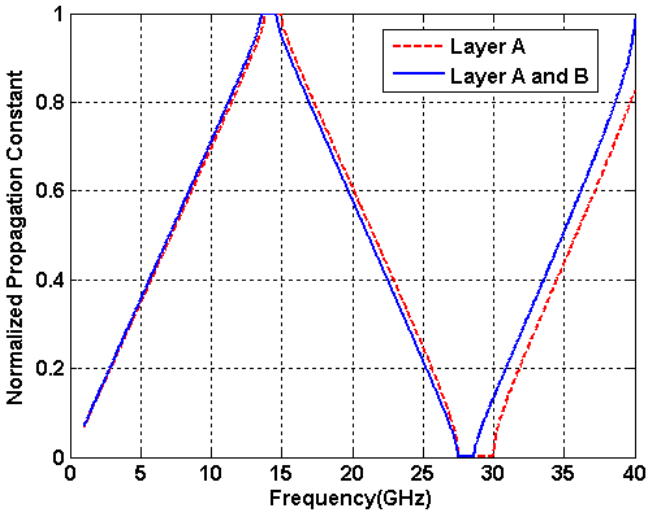

Fig. 3.19. Dispersion curve for the structure of Fig. 3.18 when modal polarization matches the dipoles on layer A. The solid curve in this figure illustrates the case that just layer *A* is present in Fig 3.18, while the dashed curve represents the case that both layers *A* and *B* are present

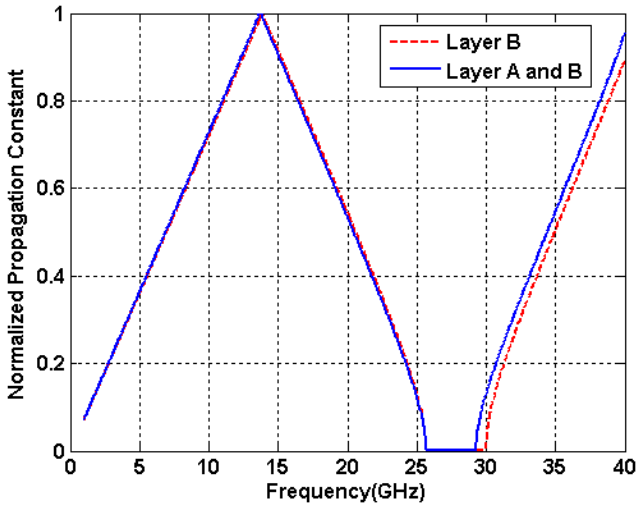

Fig. 3.20. Dispersion curve for the structure of Fig. 3.17 when modal polarization matches the dipoles on layer A. The solid curve in this figure illustrates the case that just layer *A* is present in Fig 3.17, while the dashed curve represents the case that both layers *A* and *B* are present

Subsequently, simulations were carried out to study the effect of polarization parallel to the dipoles on layer *B* and the results are shown in Fig. 3.20.

There is only one band gap around 30 GHz within the simulated frequency band and the bandgap turns out to be wider than the bandgap of the dispersion characteristic shown in Fig. 3.18 around this same frequency. There is no bandgap around 15GHz as opposed to what was observed in Fig. 3.19 for *E*-field polarization parallel to dipoles on layer *A*. Based on these simulation results, the location of stop-band and pass-band of the structure are affected by removing layer *A* when *E*-field polarization of the mode is parallel to dipoles on layer *B*, while the substrate is present. Also, dispersion curve is less affected by removing layer *A* rather than removing layer *B*, because the former has more resemblance to the structure composed of both layers.

3.7 Other Configurations: Metal Strip

Another configuration that can be considered here is the case of metal strip. In this case (as opposed to dipole) the perfect electric conductor (PEC)strip hits the boundaries of the structure, and as a result some interesting phenomena occur. The simulation results for this case are shown in Fig. 3.21 for lattice parameters of T_x=1mm, Ty=0.2mm, and the dipole parameters were l=1mm and w=0.1mm and the simulation is performed for free standing case. Single layer of the structure is highly reflective. Similar to Fabry-Perot resonators, this high reflection results in narrow pass-bands for a cascade of similar surfaces [10].

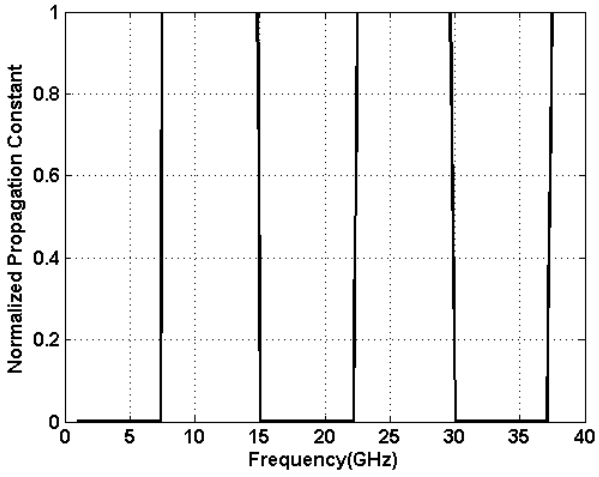

Fig 3.21 Fabry-Perot phenomena in metal strip

3.8 Conclusion

In this chapter, 1-D Photonic Band Gap structures composed of layers of dipole elements were presented and the impact of structural parameters on bandgap width and frequency were discussed in full detail. The control over the dispersion curve variation by adjusting the size of the element and/or lattice size, demonstrates the versatility of the 1-D PBG composed of dipoles for the manipulation of the dispersion characteristics.

The angular sensitivity of the structure was studied in order to determine the projected band diagram for TE and TM polarizations. Such information will allow designers to efficiently predict the dispersion properties of 1-D PBG structures.

A novel 1-D PBG structure composed of layers of dipoles with orthogonal orientation was introduced. This novel type of PBG showed simultaneous polarization and frequency selectivity that can be adjusted independently for the two orthogonal polarizations and can be used for filtering purposes.

In the coming chapter of this work, the same procedure will be repeated for the case of resonant ring elements and the results will be compared with the case of dipole.

3.9 References for Chapter 3

1. C.A. Kyriazidou, H.F. Contopanagos, W.M. Merrill, and N.G. Alexópoulos, "Artificial versus natural crystals: effective wave impedance of printed photonic bandgap materials," *IEEE Trans. Antennas Propag.*, vol. 48, pp. 95-106, 2000.
2. C.A. Moses and N. Engheta, "Electromagnetic wave propagation in the wire medium: a complex medium with long thin inclusions," *Wave Motion*, Vol. 34, pp. 301-317, 2001.
3. HFSS ver. 12. Pittsburgh, PA, Ansoft Corp.
4. R.S. Kshetrimayum and L. Zhu, "Guided wave characteristics of waveguide based periodic structures loaded with various FSS strip layers," *IEEE Trans. Antennas Propag.*, vol. 53, pp. 120-124, 2005.
5. A. Akbarzadeh-Jahromi, M. Tayarani, and M. Khalaj-Amirhosseini, "Periodically loaded rectangular wave guide with FSS Strip layer supporting wideband Backward Wave," *Int. J. Electrical, Electronics and Computer System*, vol. 04, pp. 20-23, 2011.
6. R.E. Collin, "Chapter 8: Periodic Structures and Filters," *in Foundations for Microwave Engineering*, 2nd Ed. IEEE Press, New-York, 1991.
7. A. Yariv, P. Yeh, *Electromagnetic Propagation in Periodic Media, in Optical Waves in Crystals: Propagation and Control of Laser Radiation*, Wiley, Hoboken, 2003.
8. D.N. Chigrin, and C.M. Sotomayor Torres, "Periodic thin-film interference filters as one-dimensional photonic crystals," *Opt. Spectrosc*., pp. 1-6, 2001.
9. F. Birbir, J. Shaker, and Y.M.M. Antar, "Chebishev bandpass spatial filter composed of strip gratings," *IEEE Trans. Antennas Propag.*, vol. 56, pp. 3707-3713, 2008.
10. G.R. Fowles, *Introduction to Modern Optics*, Dover Publications, New-York, 1989.

Chapter 4

Dispersion Characteristics of 1-D PBG Structures Composed of Split Ring Resonators

4.1 Introduction

Split Ring Resonators (SRRs) have been used to construct artificial material [1-6], frequency selective surfaces [7], and filters [8]. These structures can be set into a dense lattice as a result of their specific resonances. The term SRR has been used equally in the literature to refer to two concentric rings [1-6] or to an individual ring [7, 9, 10]. This individual ring is also known as open ring [11].

Following the procedure of Chapter 3, the dispersion characteristic of 1-D PBG structure composed of layers of ring element is studied in this chapter. The main difference between the 1-D PBG structure comprised of layers of open square ring element presented in this chapter and the 1-D PBG structure comprised of layers of subwavelength dipole presented in the previous chapter, is the rich resonant behaviour of open square ring, which leads to interesting phenomena in the context of 1-D PBG structures.

Resonant behaviour and current distribution of an individual ring are presented in section 4.3, and following the procedure of Chapter 3, dispersion characteristic of 1-D PBG structure composed of SRR, as a function of cell element configuration, is presented and discussed. Angular sensitivity of the same structure is also studied and the results compared with those of subwavelength dipole elements. Resonant behaviour and dispersion characteristics of coupled rings are studied in section 4.4.

4.2 Theory

The 3-D geometry and top views of the cell element of 1-D PBG structure composed of layers of Perfect Electric Conductor (PEC) SRRs are shown in Fig. 4.1. The layers are D apart along the longitudinal z-axis and T is the size of the square lattice in the transverse xoy

plane. The outer length of the ring, its width and gap size are represented by *l*, *w*, and *g*, respectively. Throughout this chapter, the following structural parameters are chosen, unless otherwise specified: *T*= 5mm, *l* = 4.5mm, *w* = 1mm and *g*= 0.5mm. Also, all simulations were performed for free standing case.

To calculate the dispersion characteristic of the 1-D PBG structure, scattering parameters of a single layer of rings were calculated using HFSS [12]. Master and slave boundary conditions along with Floquet port excitation were used to capture the periodic lattice of a single layer and plane wave excitation.

It is assumed that the separation between layers is large enough to avoid coupling through higher order Floquet modes. Transmission matrix elements of the single layer are then obtained from the knowledge of the scattering matrix of that same single layer. Then, the dispersion characteristic of the 1-D PBG structure is derived using the transmission matrix of a single layer as described in previous chapters.

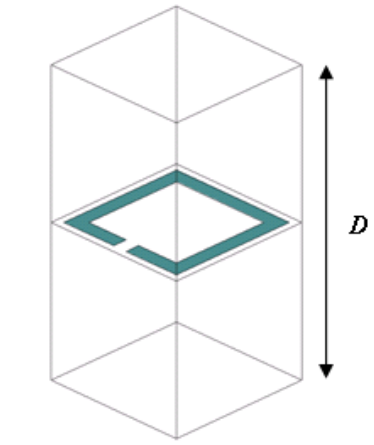

(a)

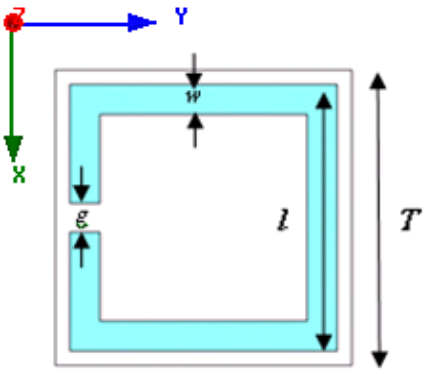

(b)

Fig. 4.1. (a) Three dimensional geometry of single cell of the PBG structure. (b) Top view of the PBG structure in the transverse plane.

4.3 Individual Ring

4.3.1 Resonance behaviour, Ring Current and dispersion characteristic

As mentioned in [7], SRR exhibit different responses depending on the polarization of the incident EM wave. For normal incidence case (Electric field in the plane of SRR and *k* vector perpendicular to the plane of SRR and parallel to the *z*-axis), two different configurations can be discerned for *E* and *H* field excitation. The field components of the first one are E_y (Electric field normal to the gap) and H_x while the other has E_x (Electric field parallel to the gap) and H_y as its field components. In the first configuration, an electric resonance is excited in SRR, which depends on the length of side part of SRR (*l*), and the resonant frequency is increased by decreasing *l.* In the second configuration, because of the asymmetry of the SRR in the direction of *E*, a magnetic resonance is excited in the ring. This magnetic resonance is resulted from a circulating current induced by the external electric field and is called the electric excitation coupling to the magnetic resonance (EEMR) [7].

In [7], it has been shown that SRRs exhibit higher order excitation modes. For the incident wave perpendicular to the plane of a single layer of SRR, one can find successive resonances in the transmission coefficient. To verify the above statement, two configurations (*E* field parallel or normal to the gap) are studied and two different behaviours are observed for transmission coefficient. For the *E* field parallel to the gap, two successive resonances are located at 10.4 GHz and 28.7 GHz (Fig 4.2-a), while for *E* field normal to the gap, one resonance can be found in transmission coefficient at 21.45 GHz (Fig 4.2-b).

Fig. 4.3 shows the current distribution for the lowest two resonant modes of SRR. As Fig. 4.3-b shows, there are one maximum in the current distribution at 10.4 GHz (lower resonance), while at 28.7 GHz (upper resonance) there are three maxima in the current distribution (Fig. 4.3-c). These current distributions are reminiscent of the current distribution of a dipole for the first, second and third modes [7].

Based on the method developed in previous chapters, dispersion characteristics of 1-D PBG structure composed of layers of ring elements are calculated for two different configurations of field vectors *E* and *H* for *D*=10 mm. Figure 4.4-a shows the dispersion curve for *E* field polarization parallel to the gap, and Fig. 4.4-b shows the same for *E* field polarization normal to the gap.

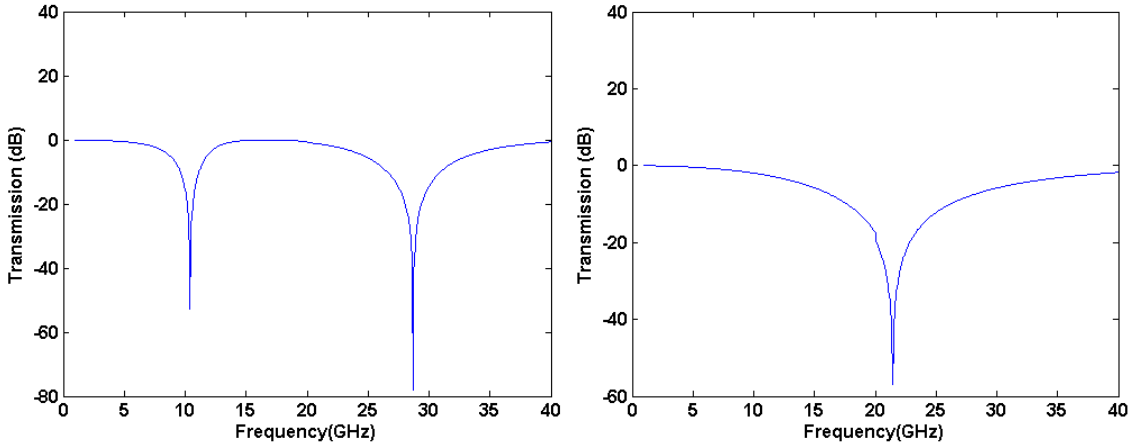

(a) (b)

Fig. 4.2. Transmission coefficient for individual ring (a) *E* field parallel to the gap (b) *E* field normal to the gap

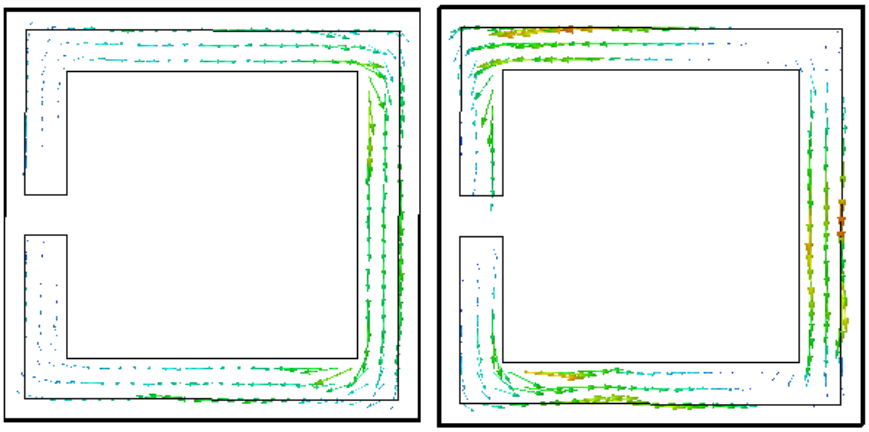

(a) (b)

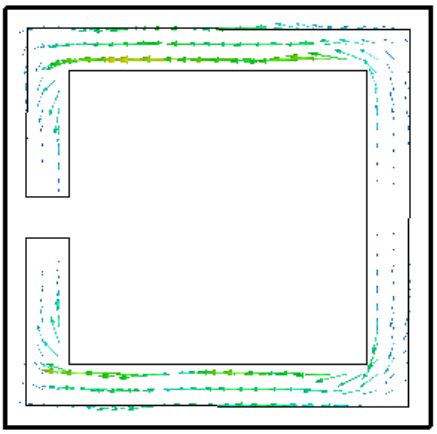

(c)

Fig. 4.3 Current distribution for *E* field parallel to the gap at (a) 10.4GHz (b) 28.7 GHz (c) *E* field normal to the gap at 21.45 GHz.

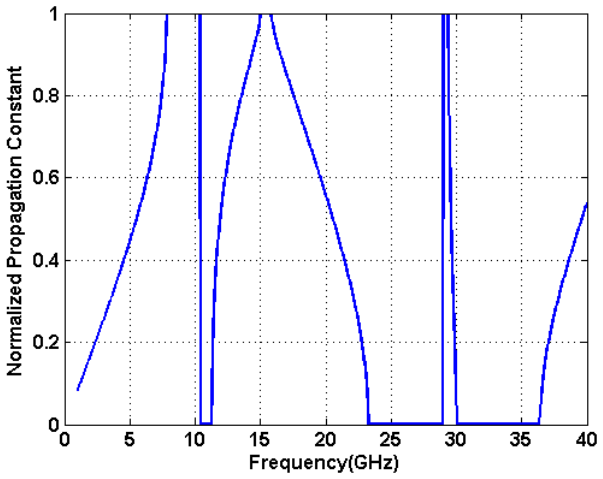

(a)

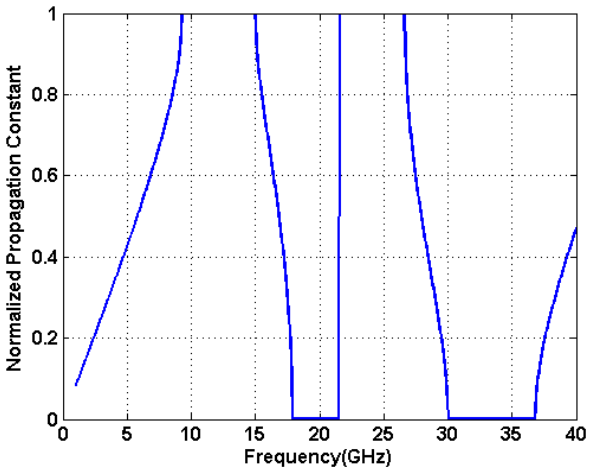

(b)

Fig. 4.4 Dispersion characteristics for 1-D PBG structure composed of ring element for (a) *E* field polarization parallel to the gap (b) *E* field polarization normal to the gap

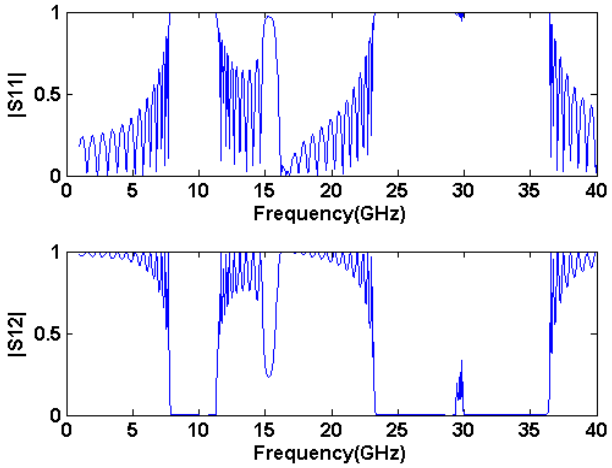

Fig. 4.5 Scattering response of the cascade of 15 layers of 1-D PBG composed of SRR for *E* field polarization parallel to the gap

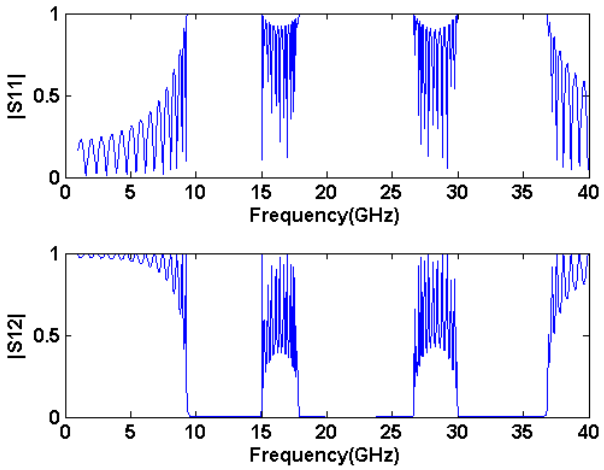

Fig. 4.6 Scattering response of the cascade of 15 layers of 1-D PBG composed of SRR for *E* field polarization normal to the gap

Like the case of 1-D PBG structure composed of dipole, the location of the structure stop-bands and pass-bands are verified using our T- matrix cascade method (Fig. 4.5 for E filed parallel to the gap and 4.6 for E filed normal to the gap). It is worth to note that, unlike the case of dipole, there is a jump in the dispersion curve of resonant ring element. This jump occurs at the resonance frequency of constituent element of the 1-D PBG layer. This is in agreement with the observations made in [13]. Beyond that, by changing the lattice parameters, and/or the angle of incidence, the resonance frequency does not change significantly. While for the case of 1-D PBGs composed of dipoles, bandgaps are formed whenever the Bragg condition is satisfied, in this case one can always come up with a bandgap around the resonance frequencies (~20 GHz for *E* field polarization normal to the gap and ~10 GHz and ~30GHz for *E* field polarization parallel to the gap) regardless of the constructive or destructive interference of the wave. This statement is further verified in the next section, in which the variations of dispersion curve vs. design parameters are studied.

4.3.2 Parametric Study

A) Dispersion characteristics as a function of cell element configuration

A set of simulations was performed to investigate the effect of the cell geometry on dispersion characteristics of the 1-D PBG structure. SRR position in space with respect to the coordinate system is shown in Fig. 4.1-b. In this set of simulations, the separation between the two consecutive layers was set at *D*=10.0 mm and the simulation was repeated for 6

different values of transverse lattice constant, T. Figure 4.7-a shows the transmission coefficient for the symmetric case (with respect to *yoz* plane), in which a normally incident plane wave with (E_y, H_x) components illuminated the structure, and Fig. 4.7-b shows the same for the asymmetric case in which a normally incident field with (E_x, H_y) components illuminates the structure. As these figures show, the resonant frequency always occurs around 10 GHz for the asymmetric case (Note that for the symmetric case, the first resonance occurs around 21 GHz, for which the simulation results are not available).

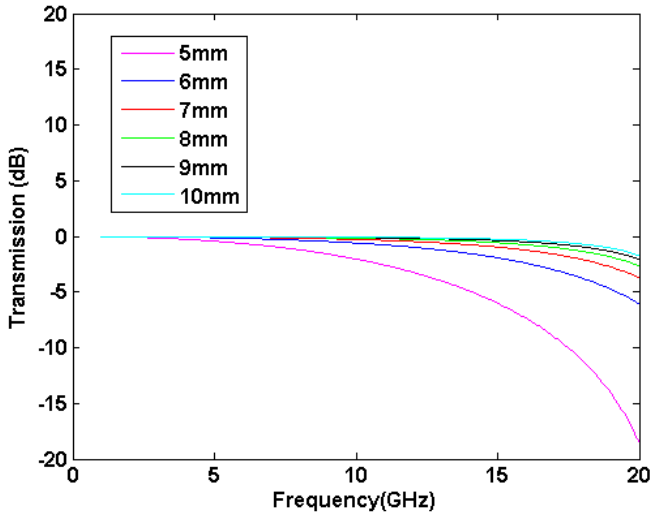

(a)

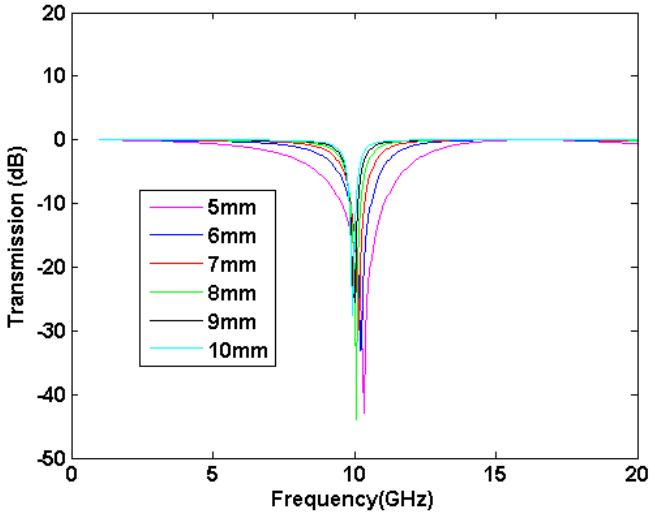

(b)

Fig. 4.7 Transmission coefficient for different cell area for (a)symmetric and (b) asymmetric case of electric field direction

The dispersion characteristics for the two different configurations are shown in Fig. 4.8. As can be seen, by increasing the cell size, the gap becomes smaller (*i.e*. the gap width decreases from 5.7 GHz to 1.5 GHz for E field polarization normal to the gap) because the PEC size becomes smaller and the structure becomes closer to the free space.

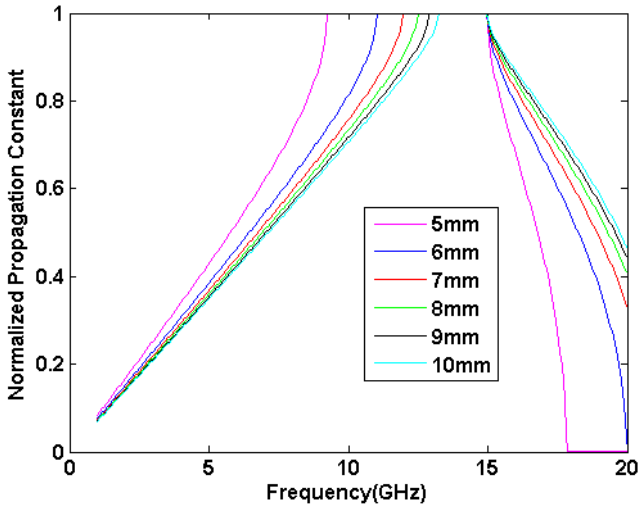

(a)

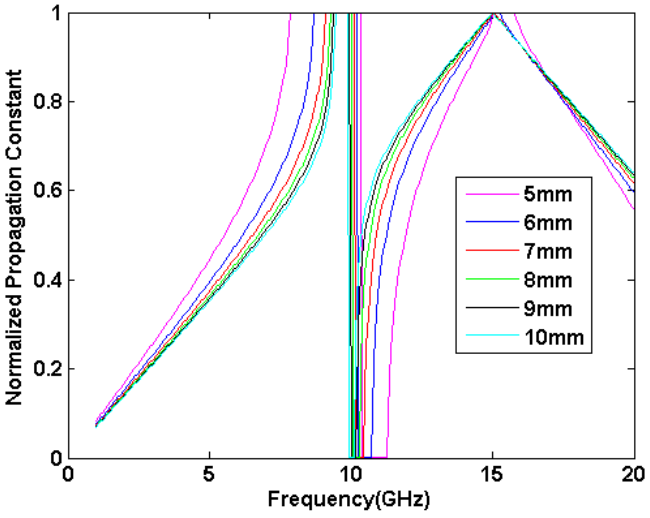

(b)

Fig. 4.8 Dispersion characteristics as a function of cell element size for (a) E field polarization normal to the gap (b) parallel to the gap

Another set of simulations was performed to examine the effect of changing the periodicity (D) on dispersion characteristics of 1-D PBG structure. The simulations were performed for three different values of D (for both configurations of E ,H, and k_z) and the results are shown in Fig. 4.9. Based on these simulation results, one can observe that by increasing the separation between the consecutive layers (D), the number of stop-bands and

pass-bands will increase. Also, the larger the separation, the smaller is the size of the bandgap.

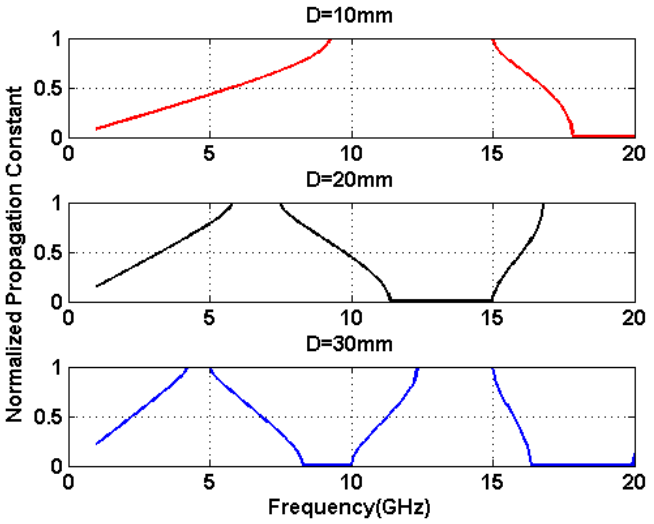

(a)

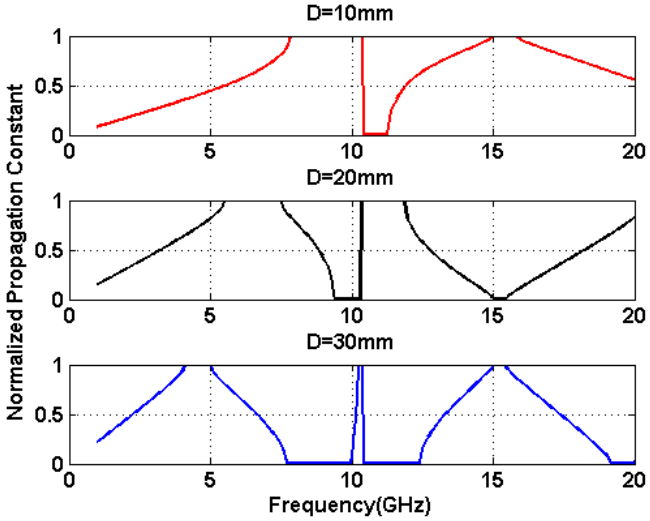

(b)

Fig. 4.9. Dispersion curve for three different separations between the consecutive layers (*D*) for (a) E field polarization normal to the gap (b) parallel to the gap

B) Angular sensitivity

As explained, SRR exhibits different responses to the incident EM wave with respect to different configurations of electric field (*E*), magnetic field (*H*) and wave vector (*k*). In the case of non-normal incidence and electric field in the plane of SRR (Fig. 4.1-b with oblique *k*), four different possibilities can be considered: TE and TM incidence in *yoz* (phi=90^{o}) and

xoz (phi=0^o) planes. It is to be noted that *xoy* plane can be defined as the transverse plane and *yoz* plane as the mirror plane (or plane of symmetry) of the structure. If the propagating angle of the mode varies in the *xoz* plane, there is strong mutual coupling between TE and TM modes, because of symmetry breakdown with respect to *xoz* plane. In this case, the summation of reflection and transmission coefficients is less than unity, and as a result, the dispersion relation (2-40) is no longer valid and proper formulation should be derived in this case, as brought in Appendix A.

In the case of oblique incidence in the *yoz* plane, the symmetry plane can be replaced by Perfect Electric Conductor -PEC- (Perfect Magnetic Conductor -PMC-) for TE (TM) incidence. The presence of the PEC (PMC) prevents coupling between polarizations and maintains similar polarizations for incident, reflected, and transmitted waves. As noted above, for the wavevector of the propagating mode in the *yoz* plane, two different TE (E_x, H_y, and H_z) and TM (H_x, E_y, and E_z) polarizations are feasible.

Based on the above argument, a set of simulations was carried out in order to investigate the variation of dispersion characteristics as the propagating angles of modes are changed. In this set of simulations, the periodicity of the structure is D=40.0mm. The angle of propagation (the angle of wavevector of the given mode of the 1-D crystal with respect to the longitudinal *z*-axis) was changed from 10^o to 60^o and transverse component, *"k_t"*, was varied accordingly to determine the dispersion characteristics using (2-40).

Figure 4.10-a shows the dispersion curve for the configuration shown in Fig. 4.1-b for the symmetric case (E_y, with k varying in the *yoz* plane), while Fig 4.10-b shows the same for the asymmetric case (E_x, with k varying in the *yoz* plane). Based on these figures, the gap shifts as the angle of propagation is increased and also the size of the gap increases by increasing the angle of incidence.

The projected band diagram, for an infinite cascade of layers composed of ring elements is depicted in Fig. 4.11-a for the TM polarization and Fig 4.11-b for TE polarization. In this diagram the transverse component of the wave vector (k_t) is calculated using (3.3).

The angular response of the structure can be then summarized in the projected band diagram for TM (H_x, E_y, and E_z) and TE (H_y, E_x, and H_z) polarizations. The normalization factor of the transverse component of the wave vector is D/π. Coloured areas of this figure correspond to propagating waves (pass-bands), while white areas indicate evanescent waves (stop-bands). A plane wave with the operating frequency and k_t in the white region of Fig. 4.9 cannot propagate through the 1-D PBG structure and will be reflected back. These high

reflection areas are strongly dependent on the angle of propagation and the frequency. It is interesting to note that the bandgap shifts to higher frequencies as the angle of propagation is increased.

What is observed in the case of 1-D PBG comprised of rings is in agreement with the observation made in the case of stratified dielectric medium and 1-D PBG comprised of dipoles, in which the size of the gap increases between the first two bands in TE polarization (as k_t is increased) as opposed to TM polarization. The difference between the 1-D PBG comprised of dipole and 1-D PBG comprised of ring is that, the gaps are significantly wider in the latter case. Also, a band gap is always observed around the resonance frequency as already mentioned.

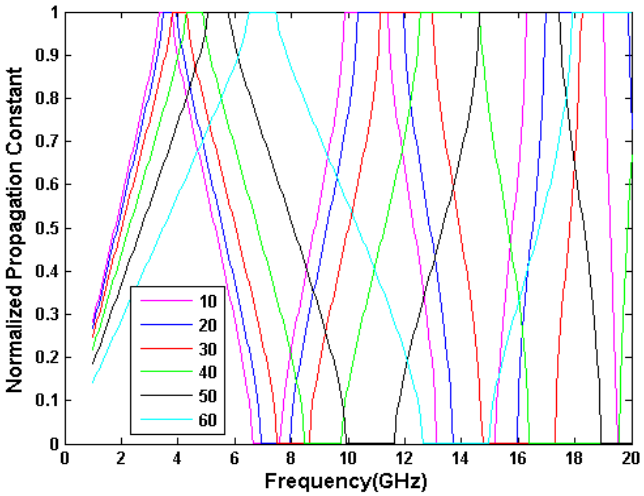

(a)

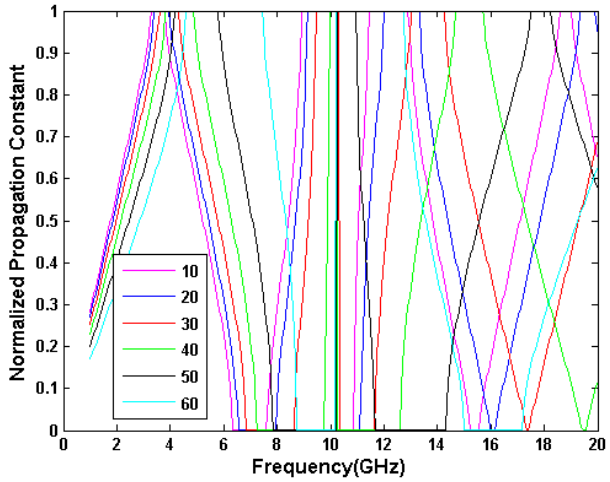

(b)

Fig. 4.10. Dispersion curves for different angle of propagations for the structure shown in Fig. 4.1-b for (a) TM polarization (b) TE polarization in *yoz* plane

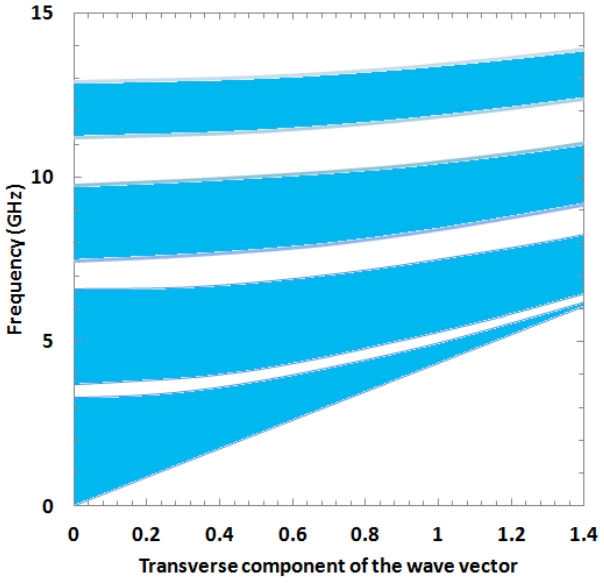

(a)

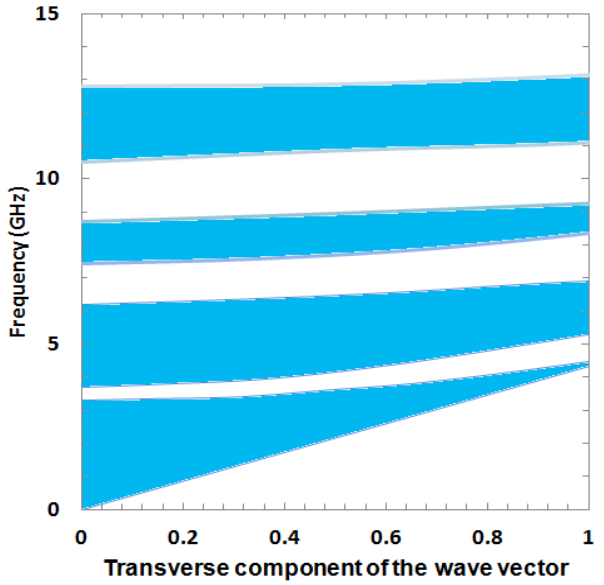

(b)

Fig. 4.11. Projected Band Diagram for the structure shown in Fig. 4.1-b for (a) TM polarization in *yoz* plane (b) TE polarization in *yoz* plane

4.4 Coupled Rings

Following the procedure of chapter 3, where the case of dipoles with orthogonal orientations within the same structure was studied, dispersion characteristics of the structure comprised of rings of different orientations is addressed in this section. The current

distribution on the rings will be presented to gain a better understanding of the underlying physical phenomenon.

A configuration composed of cell elements of two rings with either 180^o or 90^o rotations with respect to each other are studied and current distributions are investigated at reflection resonance of the single layer of each structure. The separation between the rings in the transverse plane is 5mm and the longitudinal periodicity of the structure (D) is 10mm throughout this section.

4.4.1 180^o Rotation

Two coupled rings rotated by 180^o with respect to each other are shown in Fig. 4.12. Figure 4.12-a shows the configuration in which the electric field is normal to the gap, while Fig. 4.12-b shows the case of electric field parallel to the gap (red vectors). The simulated transmission coefficient for E field polarization normal to the gap (E_y) is illustrated in Fig 4.13. As this figure shows, the resonance frequency is located at 21.6 GHz, which is around the same frequency for the E field normal to the gap for an individual ring. Figure 4.14 shows the current distribution at the resonance frequency, which shows strong current distribution in lower ring due to the fact that, by exciting the structure from the lower wave port, all the incident electric field is reflected back from the lower ring and strong current is excited on that same ring.

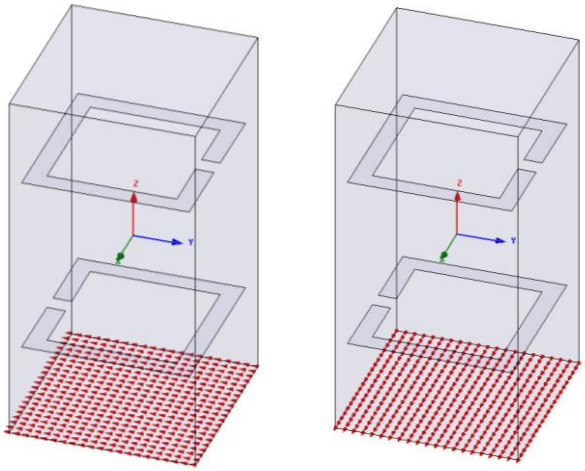

(a) (b)

Fig. 4.12 Electric field direction (a) normal to the gap (b) parallel to the gap

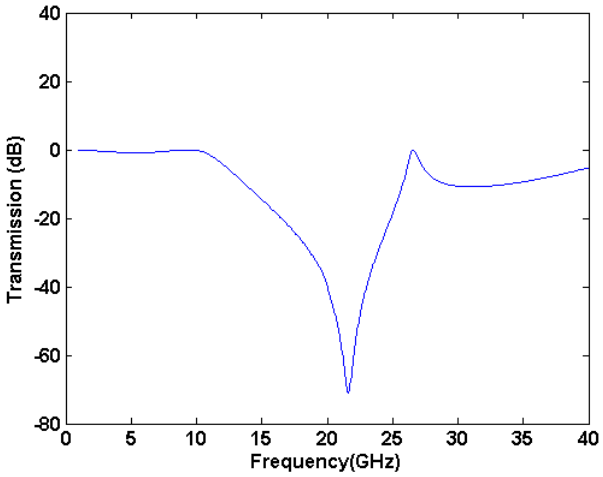

Fig 4.13 Transmission coefficient for *E* field normal to the gap

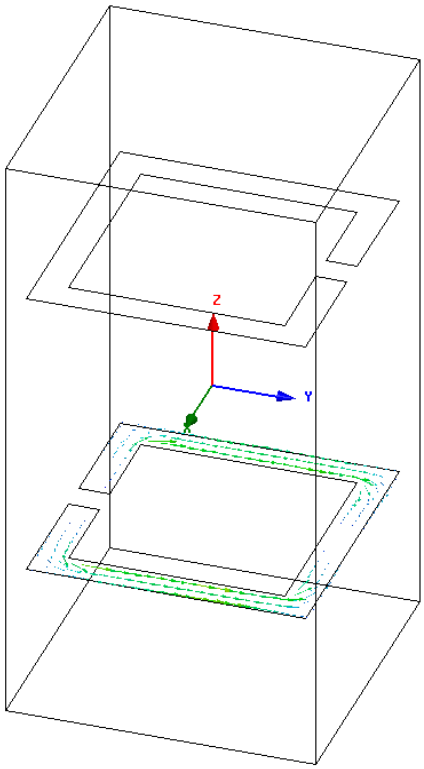

Fig 4.14 Current distribution for *E* field normal to the gap at 21.6 GHz

Figure 4.15 shows the transmission coefficient for the configuration of Fig. 4.12-b, for normal incidence with *E* field polarization parallel to the gap (E_x). As shown, two resonances occur at 10.25 GHz and 29.8 GHz, which is the same as the resonance of a layer comprised of an individual ring as its cell element and excited by electric field parallel to the gap.

The current distribution for this configuration is shown in Figs. 4.16 and 4.17 at 10.25 GHz and 29.8 GHz, respectively. It can be seen that there is a similarity between the resonant currents of the individual and coupled ring cases. Like the previous case, the lower ring has a higher current distribution.

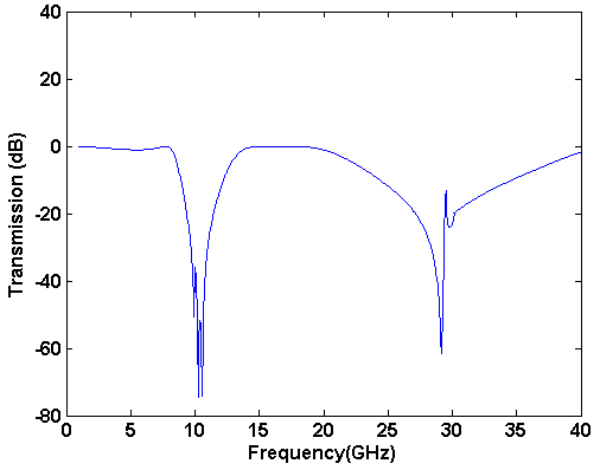

Fig 4.15 Transmission coefficient for *E* field parallel to the gap

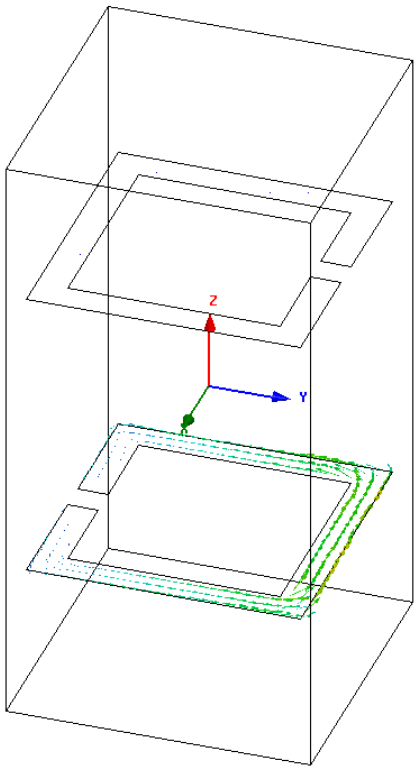

Fig 4.16 Current distribution for *E* field parallel to the gap at 10.25 GHz

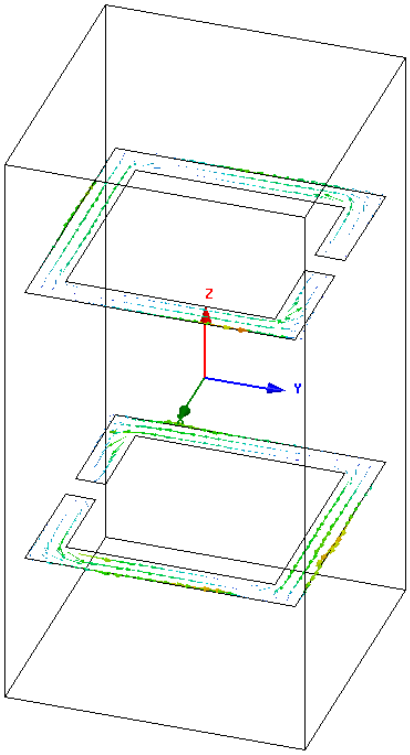

Fig 4.17 Current distribution for *E* field parallel to the gap at 29.8 GHz

Figure 4.18 shows the dispersion characteristics of the coupled ring of Fig 4.12 for the two electric field directions. There is a wide gap around 21.6 GHz for *E* field normal to the gap, while for *E* field parallel to the gap the same occurs around 10 GHz and 30 GHz. This corresponds to the resonant frequencies of the structure, as described above.

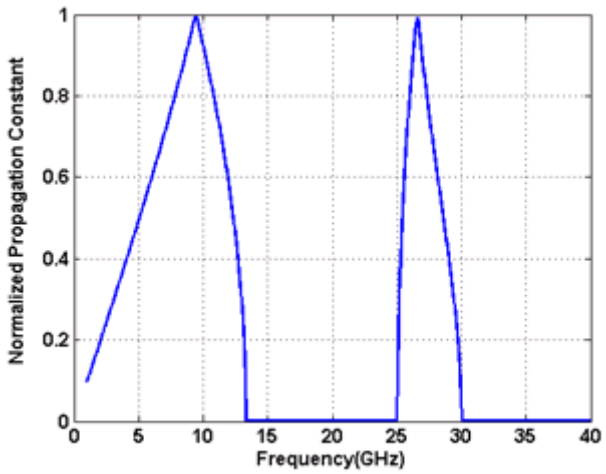

(a)

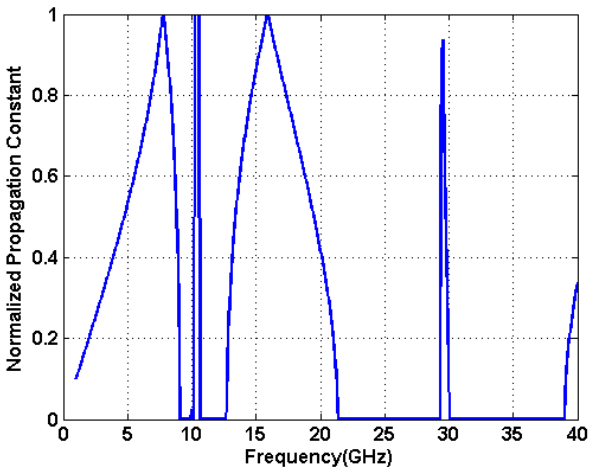

(b)

Fig. 4.18 Dispersion characteristics for 180 degree rotated rings for (a) E field normal to the gap (b) E field parallel to the gap

4.4.2 90^{o} Rotation

Another configuration consists of two rings rotated by 90^{o} with respect to each other as cell element is shown in Fig 4.19. Figure 4.20 shows the transmission coefficient for this structure, highlighting three minima at 9.95, 21.55 and 28.9 GHz.

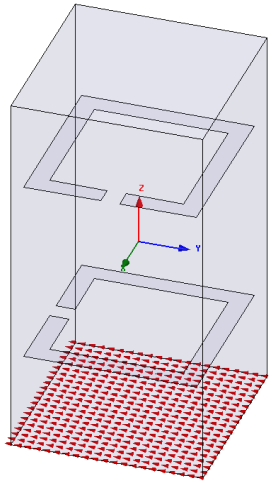

Fig. 4.19 Electric field direction with respect to the ring locations

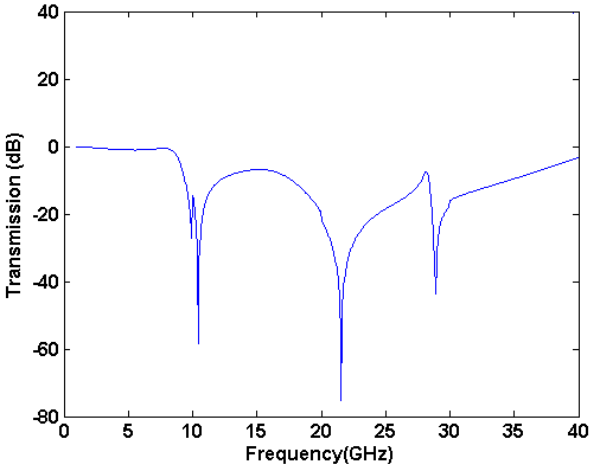

Fig 4.20 Transmission coefficient for *E* field configuration of Fig. 4.19.

Figure 4.21 shows the current distribution at the resonant frequencies of the structure shown in Fig. 4.19. As this figure shows, at first and third resonances, the upper ring has a stronger current distribution, while in second resonance the lower ring has a strong current distribution. As already discussed, for an individual ring as the cell element of the 1-D PBG and with *E* field parallel to the gap, the resonance occurs around 10 and 30GHz, while for *E* field normal the gap, the resonance occurs around 20 GHz. Based on that, the resonances of the 1-D PBG with two coupled rings (Fig. 4.21) as the cell element, correspond to the resonance frequencies of 1-D PBG's with cell elements of each of these individual ring for the same direction of the *E* field polarization.

Figure 4.22 shows the dispersion characteristics of the coupled rings displayed in Fig 4.19. As mentioned above, three resonances occur in this case (three jumps in the dispersion curve) and like the case of 180^{o} rotated rings, the dispersion curve shows wide band gaps around the resonance frequencies.

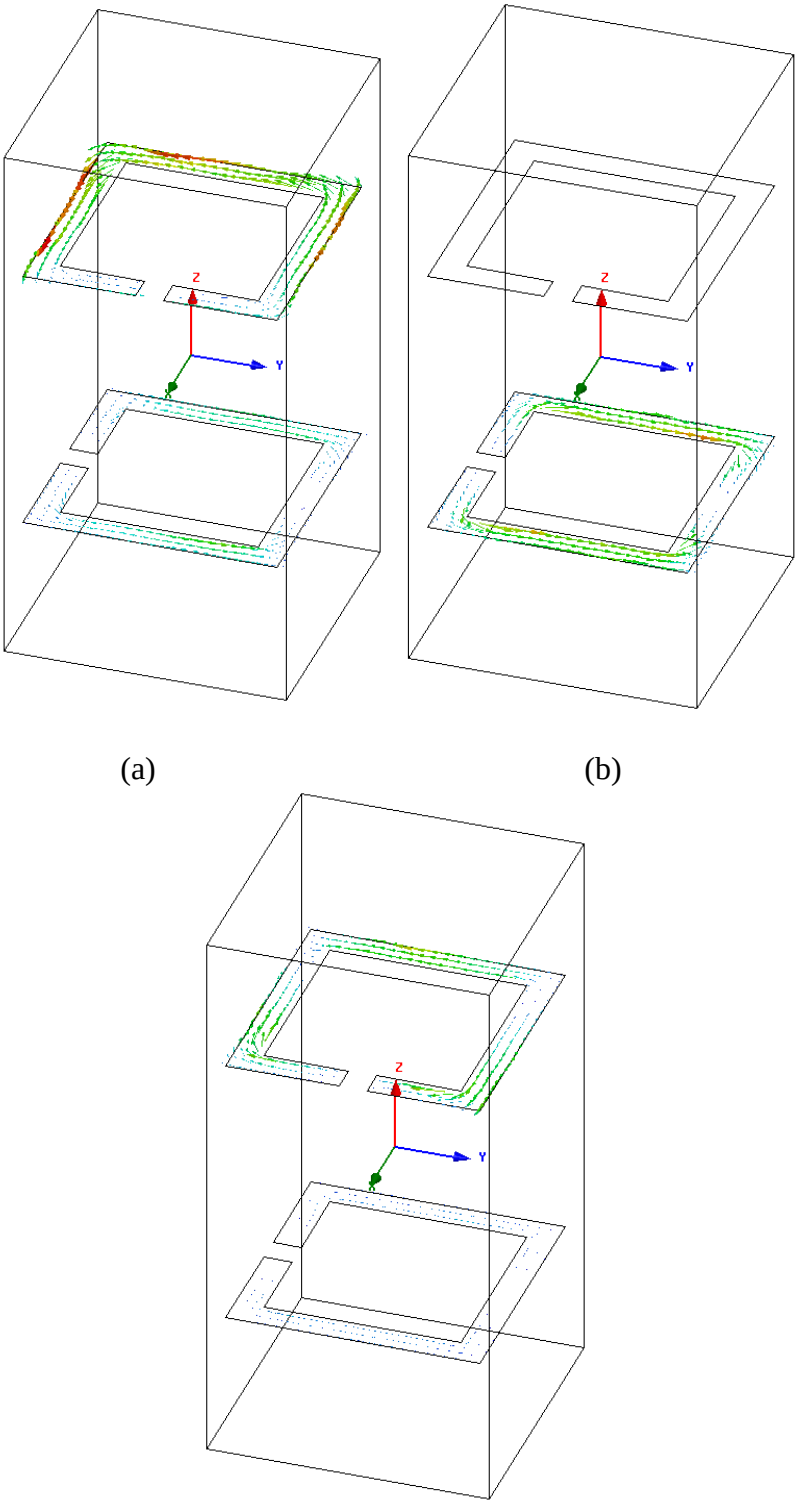

(a) (b)

(c)

Fig. 4.21: current distribution for E field polarization normal to the lower ring at (a) 9.95 GHz (b) 21.55GHz (c) 29.8GHz

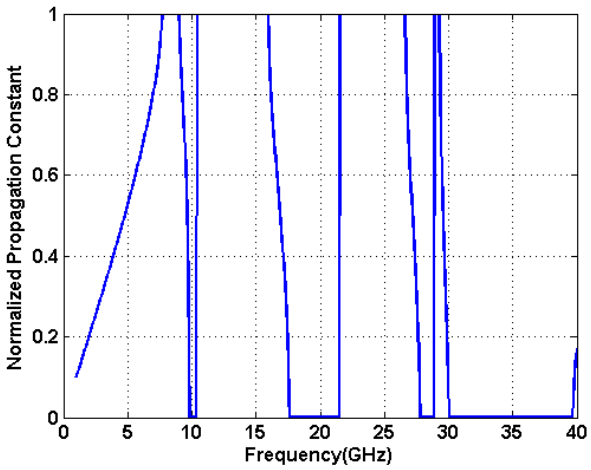

Fig. 4.22 Dispersion characteristics for 90 degree rotated rings

4.5 Conclusion

In this chapter, the resonance behavior of rings was studied and the relation between the resonance and the formation of the gap was investigated.

1-D Photonic Band Gap structures composed of SRR elements were presented and the impact of structural parameters on the width and the frequency of the bandgap were discussed in full detail.

The angular sensitivity of the structure was studied in order to determine the projected band diagram for TE and TM polarizations.

Finally, dispersion characteristics and current distribution of coupled rings were investigated for either 90 or 180 degree rotations of the ring, and the relationship between the resonance of an individual and coupled ring was investigated.

4.6 References for Chapter 4

1. D.R. Smith, J.B. Pendry, and M.C.K. Wiltshire, "Metamaterials and negative refractive index," *Science*, vol. 305, pp. 788–792, 2004.
2. C.M. Soukoulis, M. Kafesaki, and E. N. Economou, "Negative-index materials: New frontiers in optics," *Advanced Materials*, vol. 18,pp. 1941–1952, 2006.
3. S. Linden, C. Enkrich, G. Dolling, M.W. Klein, J.F. Zhou, T. Koschny, C.M. Soukoulis, S. Burger, F. Schmidt, and M. Wegener, "Photonic metamaterials: Magnetism at optical frequencies," *IEEE J. Selected Topics in Quantum Electronics*,vol. 12, pp. 1097–1105, 2006.
4. V.G. Veselago, "Experimental demonstration of negative index of refraction," *Sov. Phys. Usp*., vol.10, pp. 509, 1968.
5. J. Pendry, A. Holden, D. Robbins, and W. Stewart, "Magnetism from conductors and enhanced nonlinear phenomena," *IEEE Trans. Microwave Theory Tech*., vol. 47, pp. 2075-2084, 1999.
6. D. Smith, W. Padilla, D. Vier, S. Nemat-Nasser, and S. Schultz, "Composite medium with simultaneously negative permeability and permittivity," *Phys. Rev.Lett.*, vol. 84, pp. 4184–4187, 2000.
7. J. Zhou, T. Koschny, C.M. Soukoulis, "Magnetic and electric excitations in split ring resonators,"*Optics Express*, Vol. 15, pp. 17881-17890,2007.
8. M. Duran-Sindreu, A. Velez, G. Siso, P. Velez, J. Selga, J. Bonache, F. Martin, "Recent advances in metamaterial transmission lines based on split rings,"*Proc. of the IEEE*, vol. 99, pp. 1701-1710, 2011.
9. Z. Li *et al*., "Chiral metamaterials with negative refractive index based on four "U" shaped split ring resonator,"*App. Phys. Lett*. vol. 97, pp. 081901-081904, 2010.
10. M. Mutlu, A.E. Akosman, A.E. Serebryannikov, E.Ozbey, "Assymetric chiral metamaterial circular polarizer on four U-shaped split ring resonator,"*Opt. Lett*. vol. 36, pp. 1653-1655, 2011.
11. J. Shaker, R. Chaharmir, "Characteristics of photonic bandgap structures comprised of open square ring,"*Elect. Lett.*,pp. 1454-1455, 2010.
12. HFSS ver. 12. Pittsburgh, PA, Ansoft Corp.

13. R.S. Kshetrimayum and L. Zhu, “Guided wave characteristics of waveguide based periodic structures loaded with various FSS strip layers,” *IEEE Trans. Antennas Propag.*, vol. 53, pp. 120-124, 2005.

Chapter 5

Conclusions and Perspectives

5.1 Conclusion

In the present work, an innovative approach for characterization of one dimensional Photonic Band Gap structures comprised of metallic inclusions was presented. The steps involved in this document can be summarized as follow:

- ✓ An efficient S- to T-parameter conversion technique has been proposed to determine the dispersion characteristics of 1-D PBG structures composed of inclusions imbedded within a host medium.
- ✓ 1-D Photonic Band Gap structures composed of dipole elements were presented and the impact of structural parameters on the width and the frequency of the bandgap were discussed in full detail. The control over the variation of the dispersion curve by adjusting the size of the element and/or lattice size, demonstrates versatility of the 1-D PBG composed of dipoles for the manipulation of the dispersion characteristics.
- ✓ The angular sensitivity of the 1-D PBG structure composed of dipole elements was studied in order to determine the projected band diagram for TE and TM polarizations. Such information will allow designers to efficiently predict the properties of 1-D PBG structures.
- ✓ A novel 1-D PBG structure composed of layers of dipoles with orthogonal orientation was introduced. This novel type of PBG showed simultaneous polarization and frequency selectivity that can be adjusted independently for the two orthogonal polarizations.
- ✓ 1-D PBG structures composed of resonant open ring elements were presented and the resonant behaviour, current distribution and dispersion characteristics of a 1-D PBG composed of ring were studied. The impact of structural parameters on the width and the frequency of the bandgap were discussed in full detail and the angular sensitivity of the structure was studied in order to determine the projected band diagram. The results were compared with the case of 1-D PBGs composed of dipole elements, and

it was revealed that, as opposed to the case of dipole (in which the formation of the gap depends on the destructive or constructive interference of the waves which depends to the structural parameters), a bandgap forms in the resonance frequency regardless of the structural parameters.

- ✓ The resonance behaviour and current distribution of coupled rings were studied and relationships established between response of the individual and coupled rings.
- ✓ Dispersion characteristics of 1-D PBG composed of rings with different rotations were calculated and it was shown that a wide band gap can be achieved around the resonant frequency.

5.2 Perspectives and Future Work

This thesis work can be expanded in several other directions:

- ✓ Expanding the proposed approach to two-dimensional photonic band gap structures is for sure, the first direction to follow as future work.
- ✓ Another quite exciting direction to explore is the possible application of such work to filter design and also in modern communication systems, whenever the polarization of the incoming signal is to be used as a means of separating it from another signal in the same frequency band that is of orthogonal polarization.
- ✓ As discussed, for oblique propagation with wave vector varying in the *xoz* plane, there is a strong mutual coupling between TE and TM modes. So the dispersion relation (2-40) and the scattering matrix to transmission matrix conversion formulation (2-46) are no longer valid. Thus, the derivation given in Appendix A can be the starting point for further validation.

APPENDIX A

S- Matrix to T-Matrix Conversion for a 4 Port Network

For a 4 port network, the conversion of scattering matrix to transmission matrix element is given as the following:

$$A_{11}^{x} = \frac{a_{x1}^{+}}{a_{x2}^{+}} = \frac{S_{21}^{y}}{S_{21}^{y}S_{21}^{x} - S_{21}^{xy}S_{21}^{yx}}$$

$$A_{12}^{x} = \frac{a_{x1}^{+}}{a_{x2}^{-}} = \frac{S_{21}^{xy}S_{22}^{yx} - S_{22}^{x}S_{21}^{y}}{S_{21}^{y}S_{21}^{x} - S_{21}^{xy}S_{21}^{yx}}$$

$$A_{21}^{x} = \frac{a_{x1}^{-}}{a_{x2}^{+}} = \frac{S_{11}^{x}S_{21}^{y} - S_{11}^{xy}S_{21}^{yx}}{S_{21}^{y}S_{21}^{x} - S_{21}^{xy}S_{21}^{yx}}$$

$$A_{22}^{x} = \frac{a_{x1}^{-}}{a_{x2}^{-}} = S_{11}^{x}\left(\frac{S_{22}^{yx}S_{21}^{xy} - S_{21}^{y}S_{22}^{x}}{S_{21}^{y}S_{21}^{x} - S_{21}^{xy}S_{21}^{yx}}\right) - \frac{S_{11}^{xy}}{S_{21}^{xy}}\left(S_{22}^{x} + S_{21}^{x}\frac{S_{22}^{yx}S_{21}^{xy} - S_{21}^{y}S_{22}^{x}}{S_{21}^{y}S_{21}^{x} - S_{21}^{xy}S_{21}^{yx}}\right) + S_{12}^{x}$$

$$A_{11}^{xy} = \frac{a_{x1}^{+}}{a_{y2}^{+}} = \frac{-S_{21}^{xy}}{S_{21}^{y}S_{21}^{x} - S_{21}^{xy}S_{21}^{yx}}$$

$$A_{12}^{xy} = \frac{a_{x1}^{+}}{a_{y2}^{-}} = \frac{S_{22}^{xy}S_{21}^{y} - S_{22}^{y}S_{21}^{xy}}{S_{21}^{y}S_{21}^{x} - S_{21}^{xy}S_{21}^{yx}}$$

$$A_{21}^{xy} = \frac{a_{x1}^{-}}{a_{y2}^{+}} = \frac{S_{21}^{x}S_{11}^{xy} - S_{11}^{x}S_{21}^{xy}}{S_{21}^{y}S_{21}^{x} - S_{21}^{xy}S_{21}^{yx}}$$

$$A_{22}^{xy} = \frac{a_{x1}^{-}}{a_{y2}^{-}} = S_{11}^{xy}\left(\frac{S_{21}^{yx}S_{22}^{xy} - S_{21}^{x}S_{22}^{y}}{S_{21}^{y}S_{21}^{x} - S_{21}^{xy}S_{21}^{yx}}\right) - \frac{S_{11}^{x}}{S_{21}^{x}}\left(S_{22}^{xy} + S_{21}^{xy}\frac{S_{21}^{yx}S_{22}^{xy} - S_{21}^{x}S_{22}^{y}}{S_{21}^{y}S_{21}^{x} - S_{21}^{xy}S_{21}^{yx}}\right) + S_{11}^{xy}$$

$$A_{11}^{yx} = \frac{a_{y1}^{+}}{a_{x2}^{+}} = \frac{S_{21}^{yx}}{S_{21}^{y}S_{21}^{x} - S_{21}^{xy}S_{21}^{yx}}$$

$$A_{12}^{yx} = \frac{a_{x1}^{+}}{a_{y2}^{-}} = \frac{S_{22}^{x} S_{21}^{yx} - S_{22}^{yx} S_{21}^{x}}{S_{21}^{y} S_{21}^{x} - S_{21}^{xy} S_{21}^{yx}}$$

$$A_{21}^{yx} = \frac{a_{y1}^{-}}{a_{x2}^{+}} = \frac{S_{11}^{yx} S_{21}^{y} - S_{11}^{y} S_{21}^{yx}}{S_{21}^{y} S_{21}^{x} - S_{21}^{xy} S_{21}^{yx}}$$

$$A_{22}^{yx} = \frac{a_{y1}^{-}}{a_{x2}^{-}} = S_{11}^{y} \left(\frac{S_{21}^{yx} S_{22}^{x} - S_{21}^{x} S_{22}^{yx}}{S_{21}^{y} S_{21}^{x} - S_{21}^{xy} S_{21}^{yx}} \right) - \frac{S_{11}^{yx}}{S_{21}^{x}} \left(S_{22}^{x} + S_{21}^{xy} \frac{S_{21}^{yx} S_{22}^{x} - S_{21}^{x} S_{22}^{yx}}{S_{21}^{y} S_{21}^{x} - S_{21}^{xy} S_{21}^{yx}} \right) + S_{12}^{yx}$$

$$A_{11}^{y} = \frac{a_{y1}^{+}}{a_{y2}^{+}} = \frac{S_{21}^{x}}{S_{21}^{y} S_{21}^{x} - S_{21}^{xy} S_{21}^{yx}}$$

$$A_{12}^{y} = \frac{a_{y1}^{+}}{a_{y2}^{-}} = \frac{S_{21}^{x} S_{22}^{y} - S_{22}^{xy} S_{21}^{yx}}{S_{21}^{y} S_{21}^{x} - S_{21}^{xy} S_{21}^{yx}}$$

$$A_{21}^{y} = \frac{a_{y1}^{-}}{a_{y2}^{+}} = \frac{S_{11}^{y} S_{21}^{x} - S_{11}^{yx} S_{21}^{xy}}{S_{21}^{y} S_{21}^{x} - S_{21}^{xy} S_{21}^{yx}}$$

$$A_{22}^{y} = \frac{a_{y1}^{-}}{a_{y2}^{-}} = S_{11}^{y} \left(\frac{S_{21}^{yx} S_{22}^{xy} - S_{21}^{x} S_{22}^{y}}{S_{21}^{yx} S_{21}^{xy} - S_{21}^{x} S_{21}^{y}} \right) - \frac{S_{11}^{yx}}{S_{21}^{x}} \left(S_{22}^{xy} + S_{21}^{xy} \frac{S_{21}^{yx} S_{22}^{xy} - S_{21}^{x} S_{22}^{y}}{S_{21}^{yx} S_{21}^{xy} - S_{21}^{x} S_{21}^{y}} \right) + S_{12}^{y}$$